Full length article

Interpenetrating networks of fibrillar and amorphous collagen promote cell spreading and hydrogel stability

Lucia G. Brunel [a],[1] , Chris M. Long [b],[1] , Fotis Christakopoulos [b] , Betty Cai [b] ,
Patrik K. Johansson [b] , Diya Singhal [a] , Annika Enejder [b] , David Myung [a],[c],[d] ,
Sarah C. Heilshorn [b],[2],*

[a] *Department of Chemical Engineering, Stanford University, Stanford, CA, USA*
[b] *Department of Materials Science and Engineering, Stanford University, Stanford, CA, USA*
[c] *Department of Ophthalmology, Byers Eye Institute, Stanford University School of Medicine, Palo Alto, CA, USA*
[d] *VA Palo Alto Health Care System, Palo Alto, CA, USA*

ARTICLE INFO

ABSTRACT

Hydrogels composed of collagen, the most abundant protein in the human body, are widely used as scaffolds for tissue engineering due to their ability to support cellular activity. However, collagen hydrogels with encapsulated cells often experience bulk contraction due to cell-generated forces, and conventional strategies to mitigate this undesired deformation often compromise either the fibrillar microstructure or cytocompatibility of the collagen. To support the spreading of encapsulated cells while preserving the structural integrity of the gels, we present an interpenetrating network (IPN) of two distinct collagen networks with different crosslinking mechanisms and microstructures. First, a physically self-assembled collagen network preserves the fibrillar microstructure and enables the spreading of encapsulated human corneal mesenchymal stromal cells. Second, an amorphous collagen network covalently crosslinked with bioorthogonal chemistry fills the voids between fibrils and stabilizes the gel against cell-induced contraction. This collagen IPN balances the biofunctionality of natural collagen with the stability of covalently crosslinked, engineered polymers. Taken together, these data represent a new avenue for maintaining both the fiber-induced spreading of cells and the structural integrity of collagen hydrogels by leveraging an IPN of fibrillar and amorphous collagen networks.

Statement of Significance: Collagen hydrogels are widely used as scaffolds for tissue engineering due to their support of cellular activity. However, collagen hydrogels often undergo undesired changes in size and shape due to cell-generated forces, and conventional strategies to mitigate this deformation typically compromise either the fibrillar microstructure or cytocompatibility of the collagen. In this study, we introduce an innovative interpenetrating network (IPN) that combines physically self-assembled, fibrillar collagen—ideal for promoting cell adhesion and spreading—with covalently crosslinked, amorphous collagen—ideal for enhancing bulk hydrogel stability. Our IPN design maintains the native fibrillar structure of collagen while significantly improving resistance against cell-induced contraction, providing a promising solution to enhance the performance and reliability of collagen hydrogels for tissue engineering applications.

1. Introduction

Collagen hydrogels are widely used as three-dimensional (3D) scaffolds for tissue engineering and regenerative medicine applications due

to their favorable material and cell-interactive properties. As the most abundant protein in the human extracellular matrix (ECM), collagen comprises approximately 25 % of the body's total protein content by dry weight [1]. Its inherent biocompatibility and minimal risk of immune

---

rejection, particularly in the form of atelocollagen, make it a clinically viable material for medical implantation [2,3]. Additionally, the fibrillar structure of collagen type I and its numerous ligand-binding sites promote cell adhesion and interaction, thereby directing essential cellular behaviors including spreading, migration, and differentiation [4–6]. The ability of collagen hydrogels to closely mimic the native ECM provides a significant advantage over synthetic hydrogels, supporting more natural cellular functions and superior tissue regeneration outcomes.

Native tissues in the human body are active and dynamic biomaterials, experiencing constant interactions between the living cells and the non-living polymeric matrix in which the cells are embedded [7–9]. In particular, cells can exert forces and remodel the matrix as they undergo key cellular processes such as spreading, proliferation, and migration [10–12]. A significant drawback of collagen hydrogels is their tendency to contract over time in response to forces from contractile, encapsulated cells that exert significant tensions on the surrounding collagen fibers as they actively remodel the matrix [13–15]. This contraction presents several challenges for tissue engineering applications. For example, it can lead to instability of the engineered gels, causing substantial shrinkage and deformation of the gel shape and size. These structural changes can disrupt the gel's alignment with patient-specific geometries, reduce porosity, and alter cell density, which impacts cell viability, differentiation, and overall tissue function [16,17]. Additionally, gel contraction can hinder the efficacy and engraftment potential of engineered tissue by causing detachment from the intended implantation site [18]. This phenomenon has been observed across a variety of cell types, including fibroblasts and mesenchymal stromal cells, with the severity of contraction increasing with the time in culture [17,19,20].

Chemical crosslinkers such as glutaraldehyde, 1-ethyl-3-(3-dimethyl aminopropyl) carbodiimide hydrochloride (EDC), and N-hydroxysuccinimide (NHS) are effective in forming covalent bonds to strengthen the bulk properties of collagen hydrogels and reduce gel deformation, but their cytotoxicity and off-target effects render them less suitable for encapsulating live cells within the hydrogels during crosslinking [21–23]. These techniques therefore commonly rely on seeding cells on top of prefabricated, porous scaffolds after crosslinking [24,25]. Seeding cells on top of scaffolds can limit the homogeneity of the cell distribution, especially as the thickness of the scaffold increases. Therefore, cell-friendly crosslinking approaches have been developed that allow cells to be directly and homogeneously mixed within hydrogel precursor solutions before scaffold formation [26].

Strain-promoted azide-alkyne cycloaddition (SPAAC) click chemistry offers a covalent, bioorthogonal crosslinking strategy that avoids the cytotoxic catalysts, side-reactions, and harmful byproducts often associated with other crosslinking methods [26,27]. By chemically modifying the collagen to contain azide functional groups, the collagen can be crosslinked with a molecule containing strained alkynes, such as dibenzocyclooctyne (DBCO) [28]. SPAAC chemistry is not present in biological systems and thus non-interactive with cells, allowing cells to be encapsulated within the hydrogel precursor during crosslinking. However, unlike conventional, physically self-assembled (PHYS) collagen, SPAAC collagen does not self-assemble into a fibrillar network, a phenomenon commonly observed when using collagen solutions that are chemically modified and/or chemically crosslinked before fibrillogenesis [28–31]. Our previous studies have shown that while the covalent crosslinks in SPAAC collagen hydrogels enhance resistance against corneal cell-induced contraction, the amorphous nature of SPAAC collagen inhibits the ability of encapsulated cells to spread as they do in fibrillar microenvironments like conventional PHYS collagen [17] or the native corneal stroma [32]. As a result, new hydrogel designs are necessary to produce collagen scaffolds that provide both resistance against contraction as well as biophysical cues for cell spreading.

We hypothesized that an interpenetrating network (IPN) of collagen that incorporates both covalent crosslinking *via* SPAAC chemistry (resulting in an amorphous collagen subnetwork) and physical self-

assembly (resulting in a fibrillar collagen subnetwork) would enhance hydrogel stability against cell-induced contraction while still enabling cells to spread inside the gel. IPNs are systems composed of two or more functionally distinct polymer networks interwoven at a molecular level, yet not covalently bonded to each other. These networks allow for tuning hydrogel properties to provide biomimetic microenvironments with greater control over factors like viscoelasticity. Previous studies have explored IPNs involving collagen blended with other materials such as alginate or hyaluronic acid to achieve the desired material properties [10,33–36]. In this work, we have developed an IPN composed of collagen with two different structural forms: fibrillar and amorphous. By forming the IPN sequentially—first by allowing physical self-assembly (PHYS collagen) and then introducing the covalent crosslinking (SPAAC collagen)—we demonstrated that the resultant fibrillar network closely resembles that of unmodified, physically self-assembled collagen. Importantly, this collagen IPN successfully facilitates cell spreading, similar to PHYS collagen alone, while maintaining structural gel integrity against cell-induced contraction, similar to SPAAC collagen alone. These properties are crucial to enable cell encapsulation for *in vitro* culture or *in vivo* implantation while preserving long-term stability and function.

2. Materials and methods

2.1. Preparation of hydrogels

Preparation of PHYS collagen: Bovine type I atelocollagen solution (10 mg/mL, Advanced BioMatrix) was neutralized on ice immediately before use following instructions from the manufacturer. Briefly, 1.0 M sodium hydroxide (NaOH, Sigma), ultrapure deionized water (Millipore), and 10X phosphate buffered saline (PBS, Millipore) were added to the collagen to reach a concentration of 8 mg/mL collagen with a pH of 7.5. The solution was then diluted with cold 1X PBS to 4 mg/mL collagen. To form PHYS collagen hydrogels, the neutralized collagen solution was transferred to 8-well chambered coverslips (Ibidi, 200 μL per well) and incubated at 37 °C for 1 h for gelation.

Preparation of SPAAC collagen: Bovine type I atelocollagen solution (10 mg/mL, Advanced BioMatrix) was modified with azide functional groups using N-hydroxysuccinimide (NHS) ester chemistry to react with primary amines on collagen. To keep the collagen in solution state during the bioconjugation reaction, the entire process was performed at low temperatures (on ice or at 4 °C). First, the acidic collagen solution was neutralized on ice following instructions from the manufacturer. Azido-PEG$_4$-NHS ester (BroadPharm) was dissolved in dimethyl sulfoxide (DMSO, Fisher) at a concentration of 100 mg/mL and added to the neutralized collagen solution at 2 molar equivalents relative to primary amines on the collagen. The solution was mixed well, rotated for 2 h at 4 °C, and then dialyzed overnight in a Slide-A-Lyzer dialysis kit (3.5-kDa MWCO, ThermoScientific) against 1X PBS at 4 °C. The degree of functionalization was determined using a 2,4,6-Trinitrobenzene Sulfonic Acid (TNBSA) assay (Thermo Scientific) to quantify free amino groups, following the instructions from the manufacturer. Collagen-azide was stored at 4 °C and used within one week of the bioconjugation reaction. To form SPAAC hydrogels, collagen-azide and polyethylene glycol-dibenzocyclooctyne (PEG-DBCO, 4-arm, 10 kDa, Creative PEGworks) solutions were mixed together to reach concentrations of 2 mg/mL and 4 mg/mL, respectively. The mixture was transferred to 8-well chambered coverslips (Ibidi, 200 μL per well) and incubated at 37 °C for 1 h for gelation.

Preparation of the collagen IPN: Neutralized, unmodified collagen solution and collagen-azide solution were mixed to final concentrations of 4 mg/mL and 2 mg/mL, respectively. For simultaneous PHYS and SPAAC network formation, PEG-DBCO crosslinker dissolved in 1X PBS was added at an effective concentration of 4 mg/mL, and the solution was then transferred to 8-well chambered coverslips (Ibidi, 200 μL per well) and incubated at 37 °C for 1 h. For sequential PHYS and SPAAC

network formation, the collagen mixture without crosslinker was transferred to 8-well chambered coverslips and incubated at 37 °C for 1 h. Then, 100 μL of PEG-DBCO crosslinker dissolved in 1X PBS was added to the top of each well for an effective concentration of 4 mg/mL PEG-DBCO. Therefore, the final composition of the collagen IPN is 40 % PHYS collagen (4 mg/mL unmodified collagen) and 60 % SPAAC collagen (2 mg/mL collagen-azide + 4 mg/mL PEG-DBCO).

2.2. Mechanical characterization

Mechanical testing was performed using an ARG2 stress-controlled rheometer (TA Instruments). All measurements were confirmed to be within the linear viscoelastic regime of the materials, and representative curves were shown based on measurements of at least N = 3 independent samples.

Tests comparing PHYS and SPAAC collagen alone were conducted with a cone and plate geometry, using a 20 mm diameter and 1° angle cone, and the materials were allowed to gel *in situ* on the rheometer. All solutions were initially kept on ice, and a solvent trap or mineral oil was used to prevent evaporation during the measurement. The solutions for PHYS and SPAAC collagen were mixed at their final concentrations and immediately pipetted onto the rheometer stage. The gelation kinetics were evaluated through a temperature sweep from 4 to 37 °C (heating rate of 3 °C/min, 1 rad/s angular frequency, 1 % strain) followed by a time sweep. Once the final plateau modulus was reached, a stress relaxation test (10 % strain, 37 °C) was conducted.

Tests comparing PHYS, SPAAC, and IPN collagen were performed with an 8-mm parallel plate geometry, and the gels were formed before loading onto the rheometer. Specifically, 4 mg/mL unmodified collagen (for PHYS collagen), 2 mg/mL collagen-azide and 4 mg/mL PEG-DBCO (for SPAAC collagen), or 4 mg/mL unmodified collagen and 2 mg/mL collagen-azide (for IPN collagen) were pipetted into silicone molds (8 mm diameter, 40 μL material) and allowed to gel for 1 h at 37 °C. For the IPN collagen, PEG-DBCO dissolved in PBS was added atop the gels for a final concentration of 4 mg/mL PEG-DBCO in the gel and incubated again for 1 h at 37 °C. Gels were removed from their molds with a spatula and placed onto the rheometer stage for frequency sweeps (0.1–100 rad/s, 1 % strain, 37 °C) and stress relaxation (10 % strain, 37 °C) measurements.

2.3. UV–Vis spectroscopy

The precursor solution for SPAAC collagen gels was mixed and pipetted into a black clear-bottom 96-well plate (Costar), with 60 μL of sample per well. The absorbance was immediately read using UV–Vis spectroscopy at 310 nm to track the decay in absorbance of the acetylenes in DBCO, a common technique for monitoring the kinetics of SPAAC reactions [37]. Measurements were collected at room temperature every minute for 120 min.

2.4. Fluorescence Recovery After Photobleaching (FRAP) measurements

For Fluorescence Recovery After Photobleaching (FRAP) measurements, IPN collagen gels were formulated with or without the PEG-DBCO crosslinker. A 10-kDa fluorescein isothiocyanate (FITC)-dextran probe (Sigma) was suspended within the gels at a concentration of 1 mg/mL. 30 μL of material were loaded into a clear-bottom, half-area 96-well plate (Greiner Bio-One) and incubated at 37 °C for 1 h. FRAP experiments were performed using a STELLARIS 5 confocal microscope (Leica) with 60 s of photobleaching (110 μm x 110 μm area, 488 nm laser, 100 % intensity), followed by 120 s of acquisition time. Diffusion coefficients were calculated using the "frap_analysis" MATLAB program [38].

2.5. Enzymatic degradation assay

An accelerated degradation assay with collagenase was performed on PHYS, SPAAC, and IPN collagen gels. The gels were exposed to 1 wt% collagenase (Gibco) in PBS and incubated at room temperature on an orbital shaker. Every hour, the collagenase solution was removed to weigh the samples, and fresh collagenase was then added. The process was continued for a total of 5 h until all gels had fully degraded.

2.6. Cell culture, encapsulation, and seeding

Corneal mesenchymal stromal cells (MSCs) were isolated from a human donor cornea (Lions Eye Institute for Transplant and Research) according to established protocols [39]. The donor was between 30 and 35 years old and had no history of herpes simplex virus, varicella zoster virus, human immunodeficiency virus, or hepatitis. The death-to-preservation time was <7 days, and the cornea was provided in Optisol corneal storage medium. Cells were expanded in growth medium consisting of 500 mL MEM-Alpha (Corning), 50 mL fetal bovine serum (Gibco), 5 mL GlutaMax (Gibco), 5 mL non-essential amino acids (Gibco), and 5 mL antibiotic-antimycotic (Gibco). Growth medium was changed every other day, and corneal MSCs were passaged upon reaching 80 % confluency. The corneal MSCs were used for experiments between passages 7–9.

For cell encapsulations in 3D, the corneal MSCs were trypsinized, counted, pelleted, and re-suspended at a density of 5×10^5 cells/mL in 4 mg/mL unmodified collagen (for PHYS collagen), 2 mg/mL collagen-azide and 4 mg/mL PEG-DBCO (for SPAAC collagen), or 4 mg/mL unmodified collagen and 2 mg/mL collagen-azide (for IPN collagen). In the case of SPAAC collagen with a higher concentration of collagen-azide to match the concentration of collagen in PHYS collagen, cells were resuspended in a solution of 4 mg/mL collagen-azide and 4 mg/mL PEG-DBCO. The solutions were then pipetted into silicone molds (4 mm diameter, 10 μL material) or 18-well glass bottom chamber slides (Ibidi) (5.7 mm x 6.1 mm, 75 uL material) and allowed to gel for 1 h at 37 °C. After gelation, growth medium (for PHYS and SPAAC collagen) or growth medium with dissolved PEG-DBCO for a final concentration of 4 mg/mL PEG-DBCO in the gel (for IPN collagen) was added atop the gels. The medium was changed every other day during the duration of the culture period (5 days).

For cell seeding on top of SPAAC collagen gels in 2D, acellular SPAAC collagen was first gelled within molds as previously described. Corneal MCSs were trypsinized, counted, suspended within corneal MSC growth medium, and seeded on top of the gels with an initial seeding density of 10,000 cells/cm².

2.7. Microscopy of collagen fibrils

The fibrillar collagen networks were visualized using second harmonic generation (SHG) microscopy with an inverted microscope (Nikon, Ti2-E equipped with a C2 confocal scanning head and a Nikon CFI Apochromat TIRF 100XC oil immersion objective). The C2 scanner was augmented with a slidable mirror (Optique Peter) allowing switching between confocal fluorescence (with laser diode wavelengths 405, 488, 561, and 647 nm) and nonlinear imaging modalities. In nonlinear imaging mode, the SHG signal was generated by probing the samples with a picosecond-pulsed laser from a system (APE America Inc., picoEmerald S with 2 ps pulse length, 80 MHz repetition rate, and 10 cm⁻¹ bandwidth) consisting of a 1031 nm mode-locked ytterbium fiber laser and an optical parametric oscillator (OPO) tunable between 700 and 960 nm. The OPO wavelength was set to 797 nm and the backscattered SHG signal (at a wavelength of 398.5 nm) was separated using a set of optical filters (BrightLine 400/12 bandpass, BrightLine 390/18 bandpass, Thorlabs FESH0500 shortpass) and detected pixel-by-pixel with a photomultiplier tube (Hamamatsu, R6357). The excitation power at the sample was 35 mW.

Gels were removed from their molds and imaged in 2-well chambered coverslips (Ibidi, 1.5H cover glass thickness) with 500 μL of PBS to prevent gel desiccation. For each sample, at least 9 image z-stacks were

acquired in different areas of the gel. Each z-stack comprised of 21 slices spaced 1 μm apart, for an effective stack depth of 20 μm. To avoid boundary effects, acquired z-stacks were centered at least 30 μm deep into the gels. All images were collected at a resolution of 1024 × 1024 pixels (75.3 × 75.3 nm/pixel) with 10.8 μs/pixel dwell time.

2.8. Image analysis of collagen fibrils

The SHG image z-stacks were analyzed using a combination of the FIJI distribution of ImageJ [40] and a modified version of a MATLAB script developed by Rossen et al. [41]. The z-stacks were processed using an east shadows filter and 3D Gaussian blur filtering (σ = 1). The collagen fibrils were thresholded from the background signal using Otsu's method [42]. The resultant binary mask was then multiplied by the original processed image to effectively isolate the fibrils from the background. The fibril thickness was determined using the "Local Thickness" plugin in FIJI. The contour length, persistence length, network mesh size, and number of fibrils were determined using a MATLAB fiber-finding algorithm.

The fiber-finding algorithm used to calculate collagen fibril contour length, persistence length, network mesh size, and the number of fibrils per image was adapted from Rossen et al. [41] and implemented in MATLAB (version R2023b). This algorithm functions by (1) tracing fibrils stepwise by iteratively searching local subvolumes from a starting point until a stopping factor is reached that separates signal from void, (2) blotting out the trace to prevent repeat counting, and (3) restarting at the next starting point until all fibrils have been exhausted. A three-dimensional Gaussian point spread function (PSF) with a voxel density of $24 \times 24 \times 100$ nm^3 was generated and rescaled to match the input data voxel resolution ($75.3 \times 75.3 \times 909$ nm^3). The residuals matrix of the input data and the PSF were used for tracing fibrils due to improved clarity over the raw input data. Using iterative parameterization, a length prioritization array of [30 15 10], cone angle of 30°, and stop factor of 0.5 were found to most accurately identify fibrils for these samples and were therefore used for all analyses.

2.9. Microscopy of SPAAC collagen network

To visualize the SPAAC collagen network, all microscopy of fluorescently labeled SPAAC collagen was performed using fluorescence imaging with an inverted microscope (Nikon, Ti2-E equipped with a C2 confocal scanning head and a Nikon CFI Apochromat TIRF 100XC oil immersion objective).

To fluorescently label SPAAC collagen in acellular gels, the SPAAC and IPN collagen gels were first prepared as described in Section 2.1. After gelation, the gels were incubated in 30 μM Alexa Fluor 488-DBCO (Click Chemistry Tools) in PBS containing 1 % BSA for 1 h at 37 °C. Unreacted dye was removed by washing the gels 4 times with PBS. Gels were kept covered with aluminum foil to protect them from photobleaching before fluorescence imaging.

To fluorescently label SPAAC collagen in corneal MSC-laden gels, collagen-azide was conjugated with Alexa Fluor 647-NHS ester (ThermoFisher Scientific). 100 μg Alexa Fluor 647-NHS ester was dissolved in 10 μL DMSO and added to 500 μL collagen-azide. The solution was covered with aluminum foil to prevent photobleaching, mixed well, and rotated for 24 h at 4 °C. The solution was dialyzed in a Slide-A-Lyzer dialysis kit (7-kDa MWCO, ThermoScientific) for 3 days against 1X PBS at 4 °C to remove unreacted dye. After dialysis, this fluorescently labeled collagen-azide was mixed with non-fluorescent collagen-azide at a 1:5 ratio. This dilution of fluorescently labeled collagen-azide was then used for cell encapsulation within SPAAC and IPN collagen gels as described in Section 2.6.

2.10. Microscopy and image analysis of cells within gels

Cell viability and cell aspect ratio were determined from microscopy

performed with a STELLARIS 5 confocal microscope (Leica) combining fluorescence and confocal reflectance imaging modalities with a 10X air objective or 40X oil immersion objective. To assess the viability of the corneal MSCs on Days 0, 1, 3, and 5 after encapsulation, Live/Dead staining was conducted using calcein AM and ethidium homodimer-1 (Life Technologies), following the manufacturer's instructions. The numbers of live and dead cells were determined using FIJI, and cell viability was calculated as the number of live cells divided by the total number of cells. To quantify the cells' aspect ratio (*i.e.,* ratio of major to minor axis lengths) over time as an indication of cell spreading, confocal z-stack images of live cells (calcein AM-positive) were analyzed using CellProfiler software. The aspect ratio of each cell was determined by applying the two-class Otsu thresholding, hole removal, and watershed algorithms, followed by the removal of objects with surface areas <50 μm^2. Three z-stack images (12 slices with 10 μm spacing) taken in different regions of the sample were analyzed for each sample for both cell viability and cell aspect ratio. All images were acquired at a resolution of 1024 × 1024 pixels (180.4 × 180.4 nm/pixel).

Hydrogel contraction imaging was performed with an epifluorescent microscope (Leica Microsystems, THUNDER Imager 3D Cell Culture) with a 2.5X air objective in bright field mode. To track the contraction of the cell-laden hydrogels over 5 days, images of the gels within their original molds were taken at each time point, and their areas were measured with FIJI.

Images of the cell nuclei and F-actin were taken on an inverted microscope (Nikon, Ti2-E equipped with a C2 confocal scanning head and a Nikon CFI Apochromat TIRF) with a 100XC oil immersion objective. On Day 5 after cell encapsulation in the gels, samples were prepared for fluorescence microscopy by fixation with 4 % paraformaldehyde for 1 h, followed by 3 PBS washes for 20 min each. Cell membranes were permeabilized with 0.25 % Triton X-100 in PBS (PBST) for 1 h. Nuclei and F-actin were stained by incubation with 4′,6-diamidino-2-phenylindole (DAPI, 1 μg/mL, Thermo Fisher Scientific) and phalloidin–tetramethylrhodamine B isothiocyanate (phalloidin-TRITC, 0.2 μg/ml, Sigma-Aldrich) in PBST for 1 h at room temperature. Staining was followed by 3 PBST washes for 20 min each.

Images of the proliferation marker Ki-67 were taken on a STELLARIS 5 confocal microscope (Leica) using fluorescence imaging with a 10X air objective or 40X oil immersion objective. On Day 5 after cell encapsulation in the gels, samples were fixed, washed, and permeabilized as described above. The samples were then blocked with 5 % normal goat serum (Thermo Fisher Scientific) and 5 % bovine serum albumin (Sigma-Aldrich) for 3 h. Antibody staining was performed by first incubating samples with primary antibody (mouse anti-Ki-67, 1:400 dilution, Cell Signaling) overnight at 4 °C. This was followed by 4 PBST washes for 20 min each. Subsequently, samples were incubated with a secondary antibody (goat anti-mouse IgG Alexa Fluor 488, 1:500 dilution, Invitrogen) overnight at 4 °C. This was again followed by 4 PBST washes for 20 min each. Nuclei were stained by incubation with 4′,6-diamidino-2-phenylindole (DAPI, 1 μg/mL, Thermo Fisher Scientific) in PBST for 1 h. Staining was followed by 4 final PBST washes for 20 min each. Ki-67+ cells were quantified using a Python script that performed Gaussian blurring (σ = 1), thresholding, and colocalization of the Ki-67 signal with the DAPI nuclear signal. Colocalized Ki-67 and DAPI masks were counted as Ki-67+ cells, while DAPI masks without colocalized Ki-67 were counted as Ki-67- cells. The fraction of Ki-67+ cells was calculated as the number of cells expressing Ki-67 divided by the total number of cells.

2.11. Analysis of metabolic activity of cells within gels

The metabolic activity of corneal MSCs on Days 1 and 5 after encapsulation within PHYS, SPAAC, and IPN collagen gels was assessed with an alamarBlue assay (Invitrogen). At each time point, samples were incubated with 10 % alamarBlue reagent in growth medium for 4 h, and the resultant fluorescence was measured using a plate reader with

excitation at 560 nm and emission read at 590 nm. Acellular gels were used as baseline controls. Relative metabolic activity data for Day 5 were generated by normalizing to Day 1 fluorescence readings.

2.12. Statistical analysis

Statistical analyses were performed using GraphPad Prism (Version 9.5). The Shapiro-Wilk test was used to test for normality of data. For comparison of the amine quantity in unmodified vs. azide-modified collagen, an unpaired t-test was used. For comparisons of collagen fibrillar network microstructures and comparisons of cell aspect ratios, a one-way analysis of variance (ANOVA) with Tukey's multiple comparisons test was used. Specific details of each statistical analysis are presented in the figure captions. In all cases, $N \geq 3$ independent gels for each condition, and $p < 0.05$ was considered as statistically significant. Data are presented as mean $\pm$ standard deviation unless specified otherwise.

3. Results

3.1. Design of an interpenetrating network (IPN) of fibrillar and amorphous collagen

While collagen is a highly desirable material for 3D cell culture scaffolds, the low-stiffness fibrillar network that results from physical self-assembly makes collagen susceptible to bulk deformation and shrinkage in response to cell-generated forces. While SPAAC crosslinking of collagen mitigates this issue by increasing hydrogel stiffness and stability, amorphous SPAAC collagen on its own is not conducive to the spreading of encapsulated cells in the manner of unmodified PHYS collagen (Fig. 1). To explore this phenomenon, we prepared PHYS collagen gels by neutralizing bovine type I atelocollagen at 4 mg/mL, encapsulating human corneal cells within the collagen solution, and allowing the cell-laden collagen to incubate at 37 °C for 1 h for complete gelation and self-assembly of the fibrillar network (Fig. 1A, S1A). We observed that the fibrillar network in PHYS collagen facilitates cell spreading, a key indicator of the function of mammalian cells [43,44]. However, PHYS collagen is also susceptible to shrinkage during culture as cell-imposed forces remodel the collagen fibrils, causing them to rearrange and densify around the cells over time (Fig. S2). This remodeling process propagated to significant changes in the bulk shape and size of the hydrogels (Fig. 1A).

For the SPAAC-crosslinked collagen hydrogels (Fig. 1B), we chemically modified bovine type I atelocollagen to produce a collagen-azide solution by converting approximately 50 % of the amine groups on lysines to azide groups that can participate in SPAAC crosslinking (Fig.S3). The obscuration of lysine groups involved in collagen self-assembly [45] and introduction of side chains that may cause steric hindrance [46,47] can interfere with collagen self-assembly. Therefore, after the bioconjugation reaction, collagen-azide does not spontaneously gel on its own (*i.e.*, remains a solution; Fig.S1B), even at the neutral pH and physiological temperature that enables the fibrillar self-assembly of unmodified PHYS collagen into a gel (Fig.S1A). Upon mixing with a 4-arm PEG-DBCO crosslinker and cells, the collagen-azide is then able to undergo SPAAC chemical crosslinking with gelation on a timescale similar to the PHYS collagen (crossover point when G' = G'' in < 10 min,
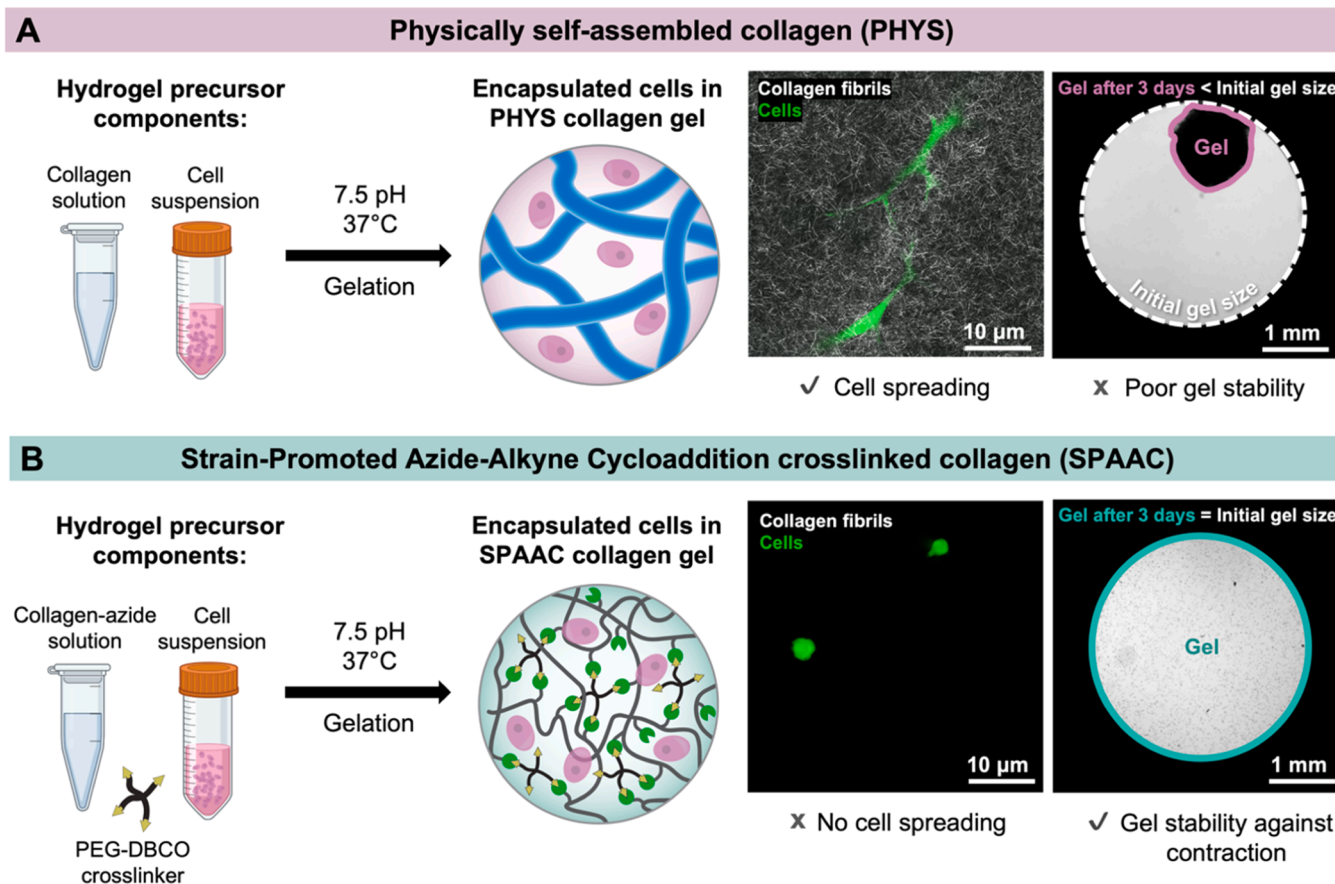

Fig. 1. Collagen hydrogels crosslinked through physical self-assembly (PHYS) or bioorthogonal covalent chemistry (strain-promoted azide-alkyne cycloaddition, SPAAC) each offer both advantages and challenges for their use as matrices for encapsulated cells. **(A)** PHYS collagen matrices are fibrillar and facilitate the spreading of encapsulated cells, but are susceptible to contraction in response to the forces exerted by encapsulated cells. **(B)** SPAAC collagen matrices do not undergo undesired contraction, but do not contain fibrils or allow cell spreading.

Fig. S1B). The consumption of the acetylenes in the DBCO as the reaction progresses is further confirmation of the SPAAC crosslinking (Fig.S1C). The covalently crosslinked SPAAC network allowed the tissue engineered construct to have robust structural stability, without shrinking or compaction. However, the cells were unable to spread effectively within the SPAAC collagen hydrogels, retaining a rounded morphology (Fig. 1B).

To address the challenge of balancing cell spreading and structural stability in collagen hydrogels, we developed an IPN that integrates two distinct structural components made from collagen: (1) a fibrillar network to support cell spreading and (2) an amorphous, covalently crosslinked network to stabilize the gel by inhibiting the long-range fibril rearrangement that causes bulk-scale contraction (Fig. 2). This IPN was formulated by combining the PHYS and SPAAC collagen
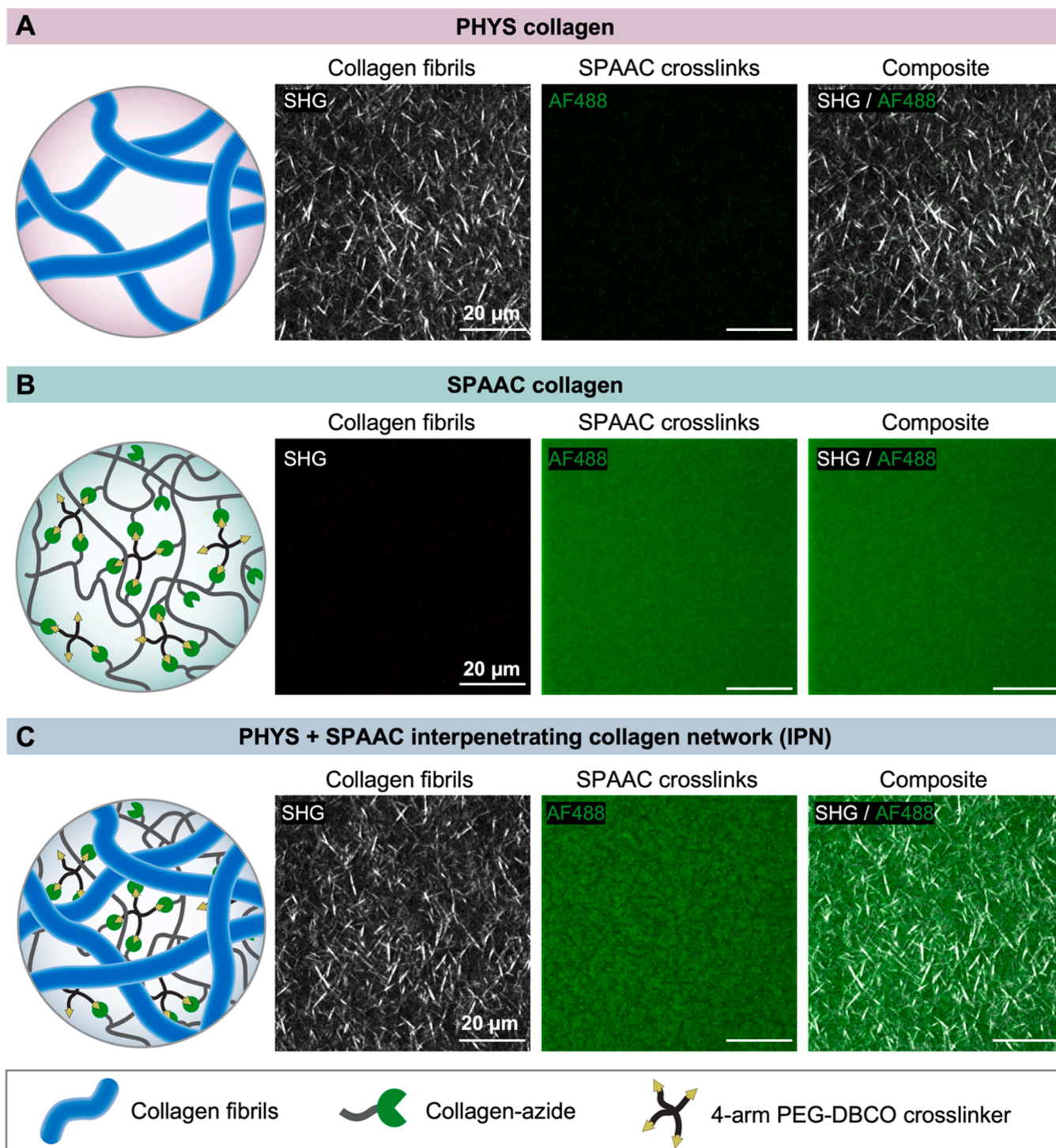

Fig. 2. Structural characteristics of the PHYS, SPAAC, and IPN collagen materials. Collagen fibrils were visualized using second harmonic generation (SHG) imaging, and the SPAAC networks were visualized using fluorescence microscopy of fluorophore-tagged collagen-azide. **(A)** PHYS collagen possesses a fibrillar network but no covalent SPAAC network. **(B)** SPAAC collagen possesses a covalent SPAAC network but no fibrillar network. **(C)** The collagen IPN contains both a fibrillar network and a covalent SPAAC network. These two signals do not appear to overlap, which suggests the fibrillar PHYS collagen and amorphous SPAAC collagen form two distinct networks.

networks (final concentrations of 4 mg/mL unmodified collagen, 2 mg/mL collagen-azide, 4 mg/mL PEG-DBCO), creating a unique hybrid hydrogel.

In its unmodified, conventional form, PHYS collagen forms a fully fibrillar network, characterized by a mesh-like arrangement of collagen struts with open voids (Fig. 2A) that traditionally facilitates cell spreading. We characterized the fibrillar network in these hydrogels using second harmonic generation (SHG) imaging. This technique takes advantage of the non-centrosymmetric structure and long-range order of collagen fibrils, allowing us to visualize the fibrillar architecture through a nonlinear optical interaction that produces a strong, characteristic signal. Through this SHG signal, we confirmed the presence of a
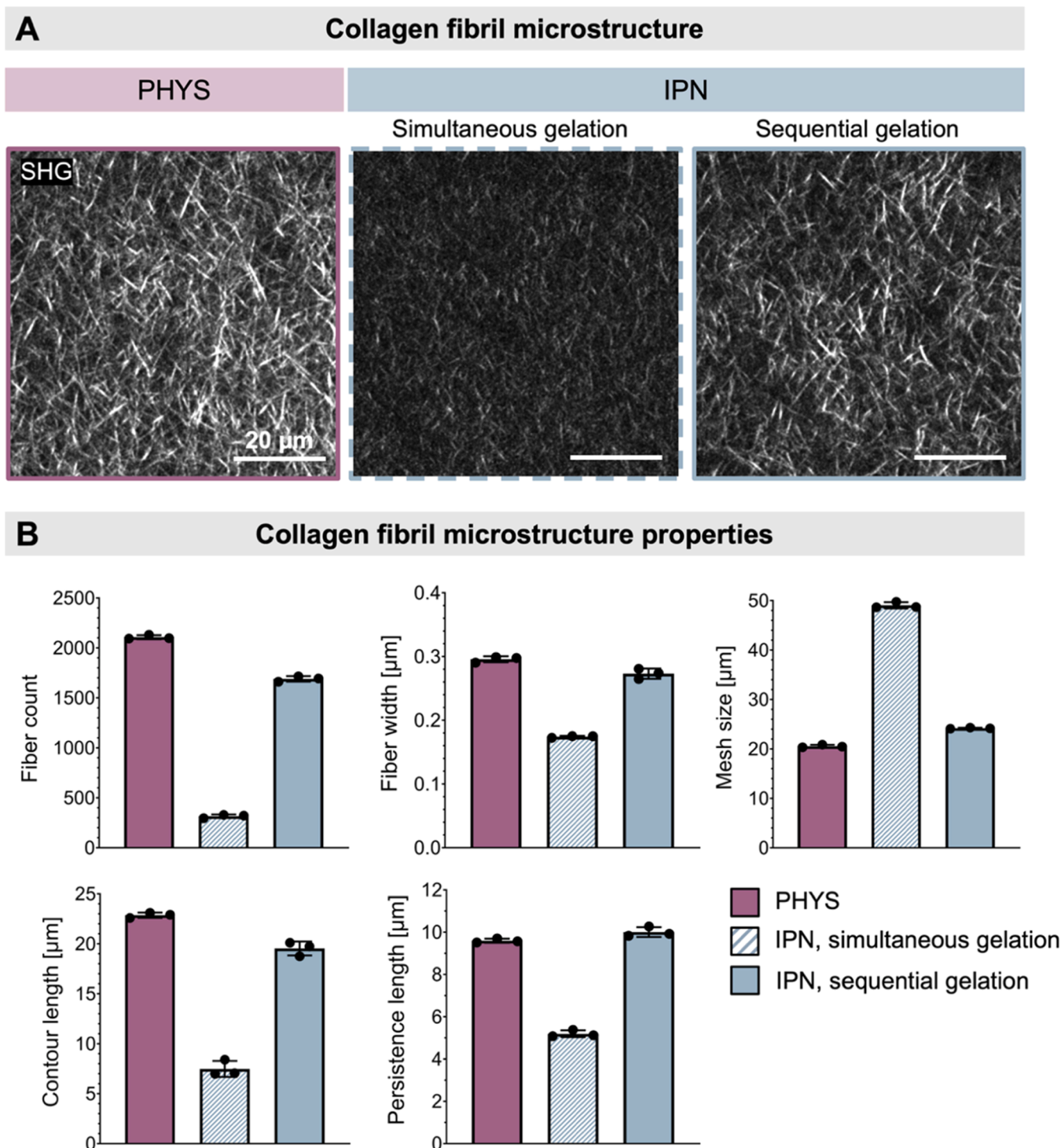

Fig. 3. Microstructural characteristics of the PHYS and IPN collagen hydrogels. **(A)** Representative SHG imaging of the PHYS collagen, the IPN collagen with simultaneous gelation of the PHYS and SPAAC networks, and the IPN collagen with sequential gelation of the PHYS and SPAAC networks. **(B)** The IPN collagen with simultaneous formation of the PHYS and SPAAC collagen networks has fewer, thinner, and shorter collagen fibrils than PHYS collagen alone. The IPN collagen with sequential formation of the PHYS network first, followed by adding the PEG-DBCO to form the SPAAC network second yields fibrils that more closely resemble those in PHYS collagen alone. N = 3 independent gels per material condition. Data plotted as mean ± SD.

well-formed fibrillar structure in PHYS collagen. In contrast, SPAAC collagen forms an amorphous, homogenous covalent network, as visualized by tagging pendant azide groups with the fluorophore Alexa Fluor 488 (AF488) after SPAAC crosslinking (Fig. 2B). Unlike other approaches of collagen crosslinking in which the crosslinking treatment is applied to the collagen after fibrillar self-assembly [23,48], the chemical modification of collagen molecules during the synthesis of collagen-azide obscures lysine amino acids while the collagen is in solution-phase. This inhibits the formation of fibrils, resulting in the observed amorphous network for SPAAC collagen gels.

By integrating PHYS collagen and SPAAC collagen together, we created a collagen IPN featuring two distinct types of collagen crosslinking and microstructures. This IPN consists of a fibrillar PHYS collagen network embedded within an amorphous SPAAC collagen network, where the SPAAC collagen completely fills the interfibrillar spaces between the PHYS collagen (Fig. 2C). When visualizing the PHYS collagen network using SHG imaging of fibrils and the SPAAC collagen network using fluorescence microscopy of AF488-tagged collagen-azide, we observed that the fluorescence signal for the SPAAC collagen was seemingly excluded from the SHG signal for the fibrillar PHYS collagen. We hypothesized that the bioorthogonality of SPAAC enables the two collagen networks to be crosslinked independently in the IPN, unlike other chemistries that may result in partial grafting of the two networks. Since collagen-azide is not amenable to physical self-assembly like PHYS collagen (Fig.S1), collagen-azide is likely not present in the collagen fibrils that self-assemble. Furthermore, since the SPAAC chemistry is absent from biology and does not nonspecifically interact with naturally occurring chemical groups, the unmodified PHYS collagen will not participate in the SPAAC reaction. In contrast to SPAAC collagen alone (Fig. 2B), the SPAAC collagen in the IPN is no longer uniformly distributed due to the presence of intervening fibrils of PHYS collagen. The spatial separation of the PHYS and SPAAC collagen networks suggests that they remain independent of each other within the IPN to form a composite structure with both fibrillar and amorphous networks coexisting.

3.2. Microstructure and mechanical properties of the collagen IPN

The IPN structure of this collagen hydrogel allows for modulation of the constituent subnetworks with control over their respective contributions to the material properties. However, because the PHYS and SPAAC collagen gels are formed by different mechanisms, they can interfere with each other during network formation. Both networks gelate under similar conditions, including a neutral pH of 7.5 and a physiological temperature of 37 °C. Given that the kinetic rates and resultant gelation times of the two networks within the IPN are similar (Fig.S1), competition between these gelation processes can occur such that the final microstructure of the material is impacted (Fig. 3). Specifically, the formation of the covalently crosslinked SPAAC collagen network can impede the self-assembly of the fibrillar PHYS collagen network. This competitive interaction results in the formation of fewer, shorter, and thinner fibrils when both networks are allowed to form simultaneously, compared to the fibrillar network observed in PHYS collagen alone (Fig. 3A).

While PHYS collagen spontaneously begins to self-assemble into a fibrous network under physiological conditions, the timing of chemical crosslinking in SPAAC collagen can be controlled by adjusting when the PEG-DBCO crosslinker is added to the solution. We hypothesized that by forming the two constituent networks of the IPN sequentially, we could prevent the interference observed in collagen fibril formation when the networks are formed simultaneously. This approach is grounded in the principles of IPN synthesis, which can occur either simultaneously or sequentially. Simultaneous IPN synthesis is the process of forming two or more polymer networks concurrently, without any of them being fully synthesized before the others begin forming. The monomers or prepolymers of each network are mixed together along with their respective initiators or catalysts, and the polymerization reactions proceed at the same time. In contrast, sequential IPNs are created either by swelling a monomer or linear polymer and crosslinker into an already-polymerized single-polymer network or by selectively crosslinking one network before the other [49–51]. The method of sequential formation can offer superior tunability and control over the hydrogel's final structural characteristics and mechanical properties [52].

In our approach to creating a collagen IPN, the PHYS collagen component is first allowed to physically self-assemble at neutral pH and 37 °C for 1 h in the presence of collagen-azide. This time window was selected based on rheometry of PHYS collagen gelation, which confirms that full gelation is achieved in <1 h (Fig.S1A). During this time, the collagen-azide solution is expected to remain stable, since the azide functional group is bioorthogonal to the unmodified collagen. Furthermore, no liquid medium is placed on top of the collagen IPN precursor during self-assembly of the PHYS collagen component, eliminating the concern of uncrosslinked collagen-azide loss due to outward diffusion.

After full gelation of the PHYS collagen in the IPN, the PEG-DBCO crosslinker is then added to initiate SPAAC crosslinking of the collagen-azide. This sequential formation of subnetworks is enabled by the diffusion of the PEG-DBCO crosslinker through the gel. The diffusivity of the crosslinker was determined by Fluorescence Recovery After Photobleaching (FRAP), both before and after the SPAAC network component of the IPN was crosslinked (Fig.S4). The crosslinking of the SPAAC network within the IPN only decreased the crosslinker diffusivity slightly, from 63 μm^2/s to 59 μm^2/s. Based on a 3D random walk diffusion model ($D = L^2/(6t)$, where D represents diffusivity, L represents distance, and t represents time), the 10-kDa PEG-DBCO molecule with a diffusivity of 59 μm^2/s will traverse the entire thickness of the hydrogel (800 μm) by random walk within 30 min. Therefore, all further characterization of the IPN collagen gels was conducted at least 1 h after introduction of the PEG-DBCO crosslinker, in order to allow for full diffusion and reaction.

The sequential gelation of the collagen IPN ensures that the fibrillar parameters—*i.e.*, contour length, persistence length, fibril width, fiber density, and network mesh size—are maintained at levels more similar to those found in PHYS collagen alone (Fig. 3B, Table S1). Although the presence of collagen-azide molecules, which do not participate in self-assembly into fibrils, has a minor effect on these properties relative to PHYS collagen alone, the overall fibrillar microstructure is largely maintained. Since this strategy of sequential network formation proved effective to preserve the fibrillar network, all subsequent work with the collagen IPN was conducted using this method to ensure consistent and optimal material properties.

To quantify the microstructural properties of the fibrillar hydrogels—the PHYS collagen and the collagen IPN—we used SHG imaging. The resultant SHG images provided high-resolution visualization of the fibrillar architecture, which we quantitatively analyzed to assess the effects of our sequential crosslinking method on fibril formation compared to the simultaneous crosslinking method and PHYS collagen alone. For this analysis, we employed a combination of the FIJI distribution of ImageJ and a modified version of a fiber-finding MATLAB algorithm originally developed by Rossen et al. [41].

This fiber finding algorithm functions by tracing lines of high-intensity pixels within a defined cone, following each line until it reaches the endpoint of a fibril. Once a fibril is fully traced, it is digitally blotted out, and the process repeats iteratively until all fibrils in the image have been characterized (Fig.S5). To optimize this process for our particular material system and images, we fine-tuned several key parameters within the algorithm, including the cone angle, the length-prioritization array, and the pixel intensity stop factor. These modifications aid in achieving accurate fibril characterization, as they avoid pathological behavior such as identified fibrils performing sharp turns at intersections or being erroneously broken up into smaller segments. Following iterative optimization, we visually confirmed that the algorithm most accurately reflected the fibrillar structure present in our

collagen hydrogels (Fig.S6).

As expected, the differences in the microstructural properties of the SPAAC, PHYS, and IPN collagen networks also result in differences in their bulk rheological properties (Fig. 4,S7). The stiffness and viscoelasticity of hydrogels are important for tissue engineering due to their effects on cell-matrix interactions and the phenotypes of encapsulated cells [53–55]. In our system, the formulations of the constituent subnetworks of the IPN (*i.e.*, PHYS and SPAAC collagen) were selected to have a similar stiffness, as described previously: G' ~ 100 Pa as measured by *in situ* rheology during the gelation process (Fig.S1). To allow for mechanical characterization of IPN collagen gels formed through sequential crosslinking of the PHYS and SPAAC collagen networks, we next conducted shear rheometry on gels that were pre-formed in molds, such that the PEG-DBCO crosslinker could be diffused into the IPN collagen gels. Similar to our previous results, the PHYS and SPAAC collagen gels alone had a similar stiffness to each other, although the magnitude was somewhat lower than with *in situ* gelation, likely due to the gel handling required to transfer the pre-formed gel onto the rheometer stage (Fig. 4A). The stiffness of the IPN collagen, which effectively combines the PHYS and SPAAC collagen subnetworks, was greater than PHYS and SPAAC collagen alone.

Gels exhibit stress relaxation when their polymer networks reorganize in response to an applied strain, thereby dissipating the internal stress over time. Conventional collagen gels exhibit characteristic stress-relaxing behavior due to the rearrangement of fibrils allowing for mechanical yielding and matrix flow [56–59]. Consistent with this characterization, we observed that PHYS collagen exhibits rapid stress relaxation (Fig. 4B). The stress relaxation half-time ($\tau_{1/2}$, time for the initial peak stress to relax to half its original value) was approximately 300 s for PHYS collagen. This rapid stress-relaxing behavior was similar across multiple concentrations of PHYS collagen (Fig.S7A), highlighting the role of the fibrillar, physically self-assembled microstructure in allowing dissipation of stress in the collagen network. In contrast, SPAAC collagen behaves like a mostly elastic gel due to the permanent, covalent crosslinks that do not allow for dynamic reorganization of the polymers ($\tau_{1/2} \sim \infty$) (Fig. 4B); this behavior was also observed across multiple concentrations of SPAAC collagen gels (Fig.S7B). When the two subnetworks of PHYS and SPAAC collagen are combined together, the collagen IPN exhibits an intermediate stress relaxation behavior ($\tau_{1/2} \sim$ 20,000 s), which is slower stress relaxing than PHYS collagen alone but faster stress relaxing than SPAAC collagen alone.

3.3. Stability of the collagen IPN against cell-induced contraction

Human corneal mesenchymal stromal cells (MSCs) were encapsulated within PHYS, SPAAC, and IPN collagen gels, remaining highly viable (>90 % viability) over 5 days in culture (Fig. 5, Table S2). Across all three material conditions, the corneal MSCs had similar metabolic activity and fraction of proliferating cells (Fig.S8).

The forces that contractile cells such as MSCs exert on their surrounding matrix can induce significant changes in the overall shape and size of the hydrogel. In particular, a challenge of conventional collagen gels is the severe densification and contraction in size that occurs as contractile cells pull on physically self-assembled collagen fibrils [13–15]. We observed that the different crosslinking mechanisms and network microstructures of PHYS, SPAAC, and IPN collagen affected the extent to which these hydrogels contracted (Fig. 6). All gels were prepared in circular 4-mm diameter molds with an initial concentration of 0.5 million corneal MSCs/mL, and the sizes of the gels were tracked daily over 5 days of culture. Due to the brightfield imaging of the gels, the fibrillar PHYS and IPN collagen gels appear darker than the amorphous SPAAC collagen gels on Day 0, since light scattering from fibrils causes opacity [60]. Over the 5-day culture period, the PHYS collagen gels with encapsulated corneal MSCs were rapidly and severely contracted. On average, PHYS collagen gels contracted to <30 % of their initial gel area within 2 days and <10 % of their initial gel area within 4 days of cell encapsulation. Since the corneal MSCs had a similar fraction of proliferating cells (Fig.S8), the higher apparent cell density for PHYS collagen gels over time (Fig. 5B) is therefore attributed to the reduction in gel area caused by PHYS collagen contraction, rather than an increase in cell proliferation. Furthermore, we observed that the PHYS collagen gels became increasingly opaque over time, consistent with collagen fiber densification during contraction [60]. In contrast, the material conditions with amorphous SPAAC collagen in the network—both SPAAC collagen alone and the IPN collagen—did not detectably contract in response to the encapsulated corneal MSCs, indicating that the amorphous, covalently crosslinked collagen network significantly increases the stability of the tissue engineered construct.

The collagen IPN has increased stability not only against cell-induced contraction, but also collagenase-mediated degradation (Fig.S9).
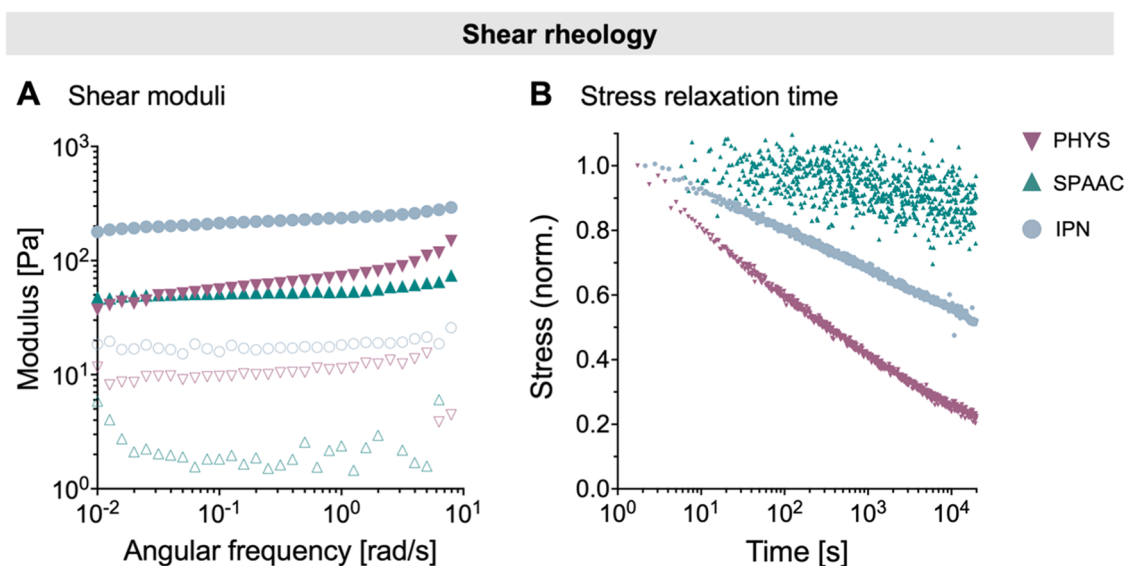

Fig. 4. Representative mechanical characterization curves for PHYS, SPAAC, and IPN collagen gels. **(A)** The constituent components of the IPN collagen, which are PHYS and SPAAC collagen, exhibit similar shear moduli to each other. When combined into the IPN network, the shear modulus increases. Filled symbols represent the storage modulus (G'), and open symbols represent the loss modulus (G"). **(B)** PHYS collagen is rapidly stress-relaxing, while SPAAC collagen does not readily stress relax. The IPN collagen relaxes slower than PHYS collagen alone but faster than SPAAC collagen alone.
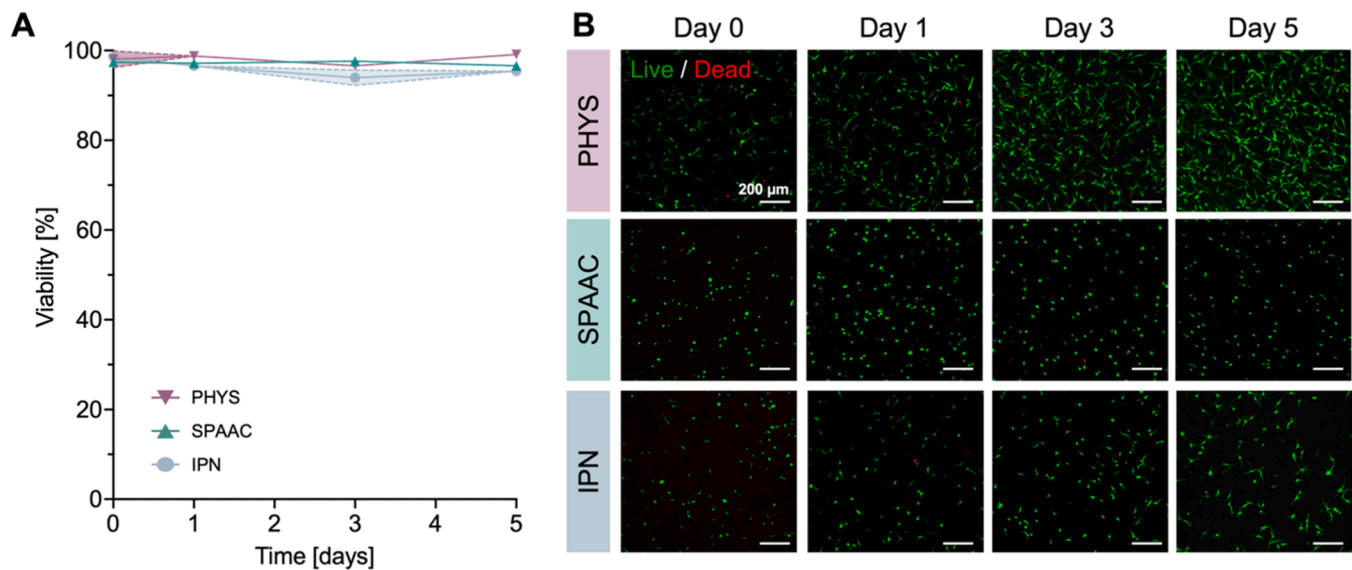
Fig. 5. Corneal MSC viability in 3D collagen gels. **(A)** Corneal MSCs encapsulated in PHYS, SPAAC, and IPN collagen remain highly viable over 5 days in culture. **(B)** Representative images from Live / Dead cytotoxicity assays of encapsulated corneal MSCs on the day of encapsulation (Day 0) and on Days 1, 3, and 5 after encapsulation. N = 3 independent gels per material condition and time point. Shaded regions represent the standard deviation from the mean.

Collagenase is found in ulcerating corneas, playing a key role in corneal collagen resorption [61]. Using an accelerated digestion test with 1 wt% collagenase, we observed that PHYS and SPAAC collagen gels degraded within 2 and 3 h, respectively. The collagen IPN achieved the greatest stability against collagenase-mediated degradation, with degradation occurring after 5 h.

3.4. Morphology of cells encapsulated in the collagen IPN

The morphology of mammalian cells is a key indicator of their function [43,44]. Therefore, understanding how cell spreading is regulated by microenvironmental cues is important for the design of biomaterials for tissue engineering [9,62,63]. In native corneal tissue, the corneal MSCs spread and elongate within the collagen-rich stroma [64,65]. We hypothesized that the presence of collagen fibrils within our IPN collagen may allow for cell spreading (Fig. 7, S10), even within a stable gel that does not experience bulk contraction (Fig. 6). Indeed, corneal MSCs were able to spread in both PHYS and IPN collagen hydrogels that contained fibrils, elongating their cell bodies and extending protrusions in multiple directions. In contrast, cells in the amorphous, covalently crosslinked SPAAC collagen alone remained rounded, extending only small protrusions (Fig. 7A). Interestingly, cells were able to spread when seeded on top of SPAAC collagen in 2D (Fig.S11), indicating that the ability of the cells to adhere to SPAAC collagen is preserved. However, the cells did not spread when encapsulated within SPAAC collagen in 3D, even when the collagen concentration was increased to match the collagen concentration in PHYS collagen gels (4 mg/mL collagen; Fig. S12). While the extent of cell spreading in the collagen IPN was initially slightly less than in PHYS collagen alone (on Days 0 and 1), the cells were able to reach and maintain the same degree of spreading in the collagen IPN as in PHYS collagen within a short timespan, by Day 3 in culture (Fig. 7B).

By imaging the fibrillar collagen IPN around the corneal MSCs over time, we observed local densification and realignment of collagen fibrils near cellular projections. The local reorganization of the collagen appeared within 24 h but then remained seemingly stable over time (Fig. S13). Corneal MSCs can therefore interact with and reorganize the collagen fibril networks in IPN collagen as the cells spread. However, while the local densification of the collagen fibrils around the cells for PHYS and IPN collagen was similar, the long-range densification of collagen that results in severe bulk contraction of the gel was observed

only for PHYS collagen and not for IPN collagen (Fig. 6). In fibrillar matrices in which the fibrils are less connected to each other, forces propagate in fewer directions and with less robust force transmission compared to highly connected networks [66]. Despite PHYS and IPN collagen having similar fibrillar microstructures (Fig. 3), we expect that the covalently crosslinked, SPAAC collagen network that fully surrounds the fibrils in the collagen IPN likely serves as a barrier between fibrils that dampens transmission of forces and inhibits long-range fibril rearrangement, thus preventing the gel from contracting. In this way, the collagen IPN allows cells to interact with collagen fibrils on a microscopic scale and adopt spread morphologies, while also maintaining a highly stable and non-contracting bulk gel structure on a macroscopic scale.

4. Discussion

A key challenge in tissue engineering is the tradeoff between allowing cells to remodel their ECM and spread while preserving the overall structural stability of the gels. Maintaining the shape and size of cell-laden hydrogels is critical for applications in personalized regenerative medicine, where precise dimensions and structural stability are necessary for implant success. This is especially challenging for tissue engineered constructs with contractile cells such as MSCs, which can exert significant forces on their surrounding matrix as they spread, leading to severe contraction of the gel. Several strategies have previously been employed to strengthen the bulk properties of collagen gels and reduce gel deformation, each with its own limitations [21,67]. For example, increasing collagen concentration enhances the mechanical properties of the gel but also alters its fibrillar structure, resulting in more, but thinner fibers that can significantly alter cell behavior [68,69]. Further, high-density collagen limits the ability of cells to proliferate, differentiate, and diffuse waste products [70]. The crosslinking of collagen with biological covalent crosslinkers like genipin has been used; however, these crosslinkers also modify the collagen microstructure and reduce the gel's pore size [71,72]. Finally, common chemical crosslinkers for collagen such as EDC/NHS and glutaraldehyde are often cytotoxic and therefore prevent the inclusion of cells within the biomaterial during crosslinking, requiring the seeding of cells on top of the scaffold rather than a homogeneous encapsulation of cells within the scaffold [21–23].

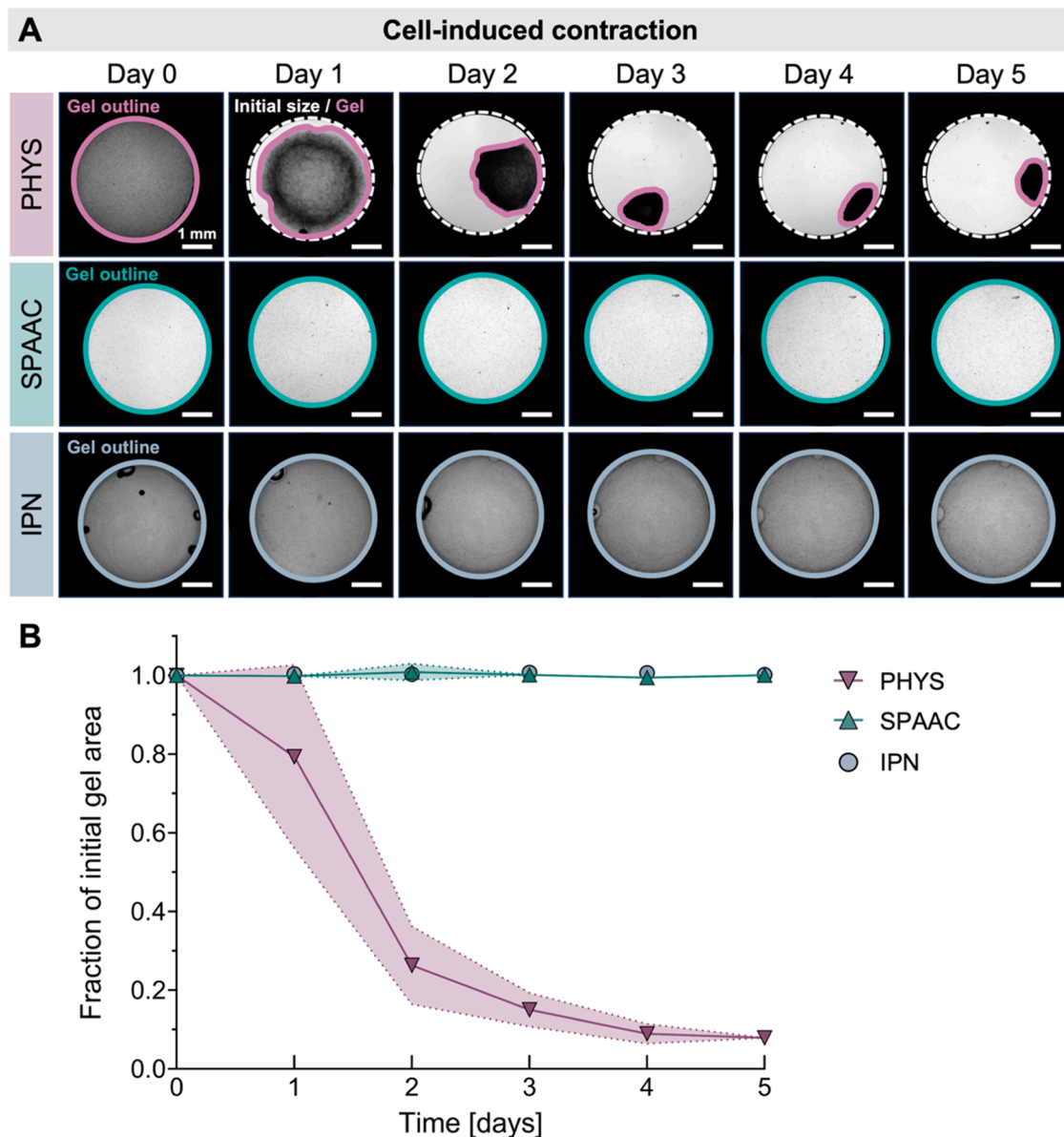Herein, we described our development of a collagen-based IPN that

Fig. 6. Stability of cell-laden PHYS, SPAAC, and IPN collagen gels against cell-induced contraction. **(A)** Representative brightfield images of gel shapes over time compared to the initial gel size. PHYS collagen with 0.5 million corneal MSCs/mL experienced severe contraction over 5 days in culture, while SPAAC and IPN collagen with 0.5 million corneal MSCs/mL did not detectably contract from their initial gel size. **(B)** Rate of collagen gel contraction. N ≥ 5 independent gels per material condition. Shaded regions represent the standard deviation from the mean.

offers the benefits of both physical self-assembly of collagen (to form a fibrillar microstructure that the cells can interact with and realign on a microscopic scale) as well as covalent crosslinking of collagen (to stabilize the bulk hydrogel on a macroscopic scale). Both networks within our IPN are based on collagen, but the different crosslinking approaches for the two networks (PHYS and SPAAC collagen) allow for a unique microstructure consisting of collagen fibrils embedded within an amorphous, covalently crosslinked collagen matrix, thus promoting both cell spreading and structural integrity simultaneously.

Our results indicate that the spreading of the human corneal MSCs is facilitated by the presence of a fibrillar collagen network. Interestingly, the cells were able to spread in the collagen IPN despite the simultaneous presence of the amorphous SPAAC collagen network, in which the corneal MSCs do not spread. Since corneal MSCs can adhere and spread over SPAAC collagen when seeded on the gels in 2D, their rounded morphologies when encapsulated in SPAAC collagen gels in 3D may be due to confinement effects [73]. In the collagen IPN, the cells may be

able to spread despite the SPAAC network due to the discontinuity in the IPN material caused by the combination of amorphous and fibrillar networks. These microinterfaces may allow cells to delaminate the bulk gel and elongate their cell bodies [74]. Cell spreading is a multifaceted process that depends on integrin clustering, focal adhesion formation, activation of intracellular signaling pathways, cytoskeletal reorganization, and mechanical interactions with the network within which the cells are encapsulated. While both fibrillar and non-fibrillar collagen present integrin binding sites, the specific presentation differs due to the supramolecular structure of fibrillar collagen [75,76]. Cell morphology has been shown to differ in response to fibrillar and non-fibrillar collagen, indicating the importance of the structural and topographical cues from the physical state of the collagen on the cell adhesion patterns, actin organization, and distribution of integrin subunits [77].

To better understand the ability of the collagen IPN to maintain structural integrity while promoting this cell spreading, our findings motivate future investigations of the propagation of a force exerted on a
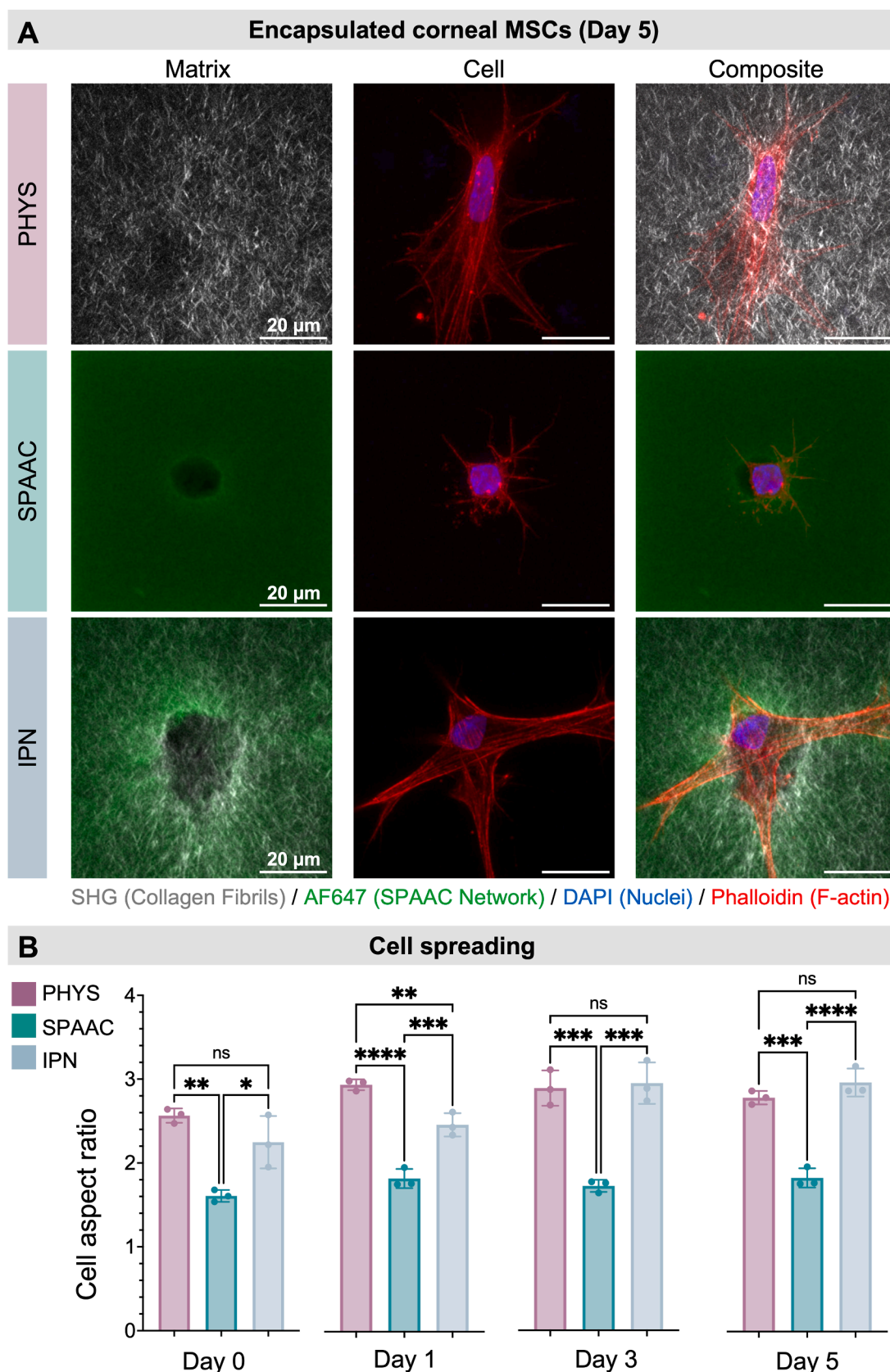
Fig. 7. Cell spreading behavior and matrix morphology. **(A)** Representative composite SHG and fluorescence microscopy images show extensive spreading of corneal MSCs in the PHYS and IPN collagen gels by Day 5 after cell encapsulation, with significantly reduced cell spreading in the SPAAC gels. **(B)** Quantification of the aspect ratios of cells in PHYS, SPAAC, and IPN collagen gels throughout the cell culture period. Statistical analyses were performed with one-way ANOVA and Tukey's multiple comparisons correction. In all cases, N = 3 independent gels per material condition and time point. Data plotted as mean ± SD. ns = not significant, * $p < 0.05$, ** $p < 0.01$, *** $p < 0.001$, **** $p < 0.0001$.

collagen fiber within an amorphous, covalently crosslinked network. In particular, our current results could be supplemented with computational modeling that considers cell-generated forces, substrate deformation, ECM density, cell migration, and proliferation [78–80]. Unlike most current models of cell-generated forces on collagen fibers, our collagen IPN is not solely fibrillar, but rather has amorphous, covalently crosslinked SPAAC collagen filling the voids between fibrils. The ability of corneal MSCs to locally rearrange collagen fibrils and spread within the collagen IPN indicates that short-range interactions between cells and collagen fibrils remain intact, facilitating essential cellular processes. Since this does not induce widespread collagen IPN gel contraction, long-range force propagation is likely inhibited by the amorphous, covalently crosslinked SPAAC collagen gel occupying the interfibrillar space, which stabilizes the overall gel structure.

Looking forward, this collagen IPN could be adapted to a variety of applications for both tissue model systems *in vitro* as well as implantable therapies *in vivo*. Cell-laden collagen hydrogels are relevant for many tissue applications including the skin, muscle, and connective tissues [81,82]. The human corneal stroma, for example, is composed of 71 % collagen by dry weight, predominantly type I collagen [83]. This collagen matrix is crucial for the cornea's biomechanical properties, and it provides a suitable extracellular microenvironment for keratocytes—specialized fibroblasts in the cornea that elongate their cell bodies between lamellae of collagen fibrils—and the corneal MSCs from which the keratocytes are derived [84,85]. Corneal MSCs can be readily harvested and expanded, and they are known to play a crucial role in regenerating corneal tissue after damage or disease [64,65,86,87]. Therefore, collagen gels laden with corneal MSCs may have potential to address the global shortage of donor corneas required for allograft transplantation to treat corneal blindness.

Generally, tissue applications for which this collagen IPN would be most advantageous are those in which the engineered scaffold must permit cells to spread and form networks while remaining mechanically robust. In addition to corneal tissue—the exemplary application described here—other cell types and tissues of interest may include fibroblasts for engineered skin, skeletal muscle cells for engineered muscle, and cardiomyocytes for engineered heart tissue [88–90]. In the human body, these collagen-rich organs contain contractile cells with dynamic behaviors. Therefore, tissue engineering approaches require a scaffold that permits dynamic cell spreading and local matrix reorganization while preserving bulk structural stability of the tissue model or implant. Based on the cell type and downstream application, the concentrations and ratios of PHYS and SPAAC collagen within the IPN may be varied to tune the material properties. For each target tissue, one can first select a total concentration of collagen that results in the appropriate matrix stiffness. For example, we have previously demonstrated that engineered matrix stiffnesses between 100 and 1000 Pa are suitable for corneal tissue engineering; this typically corresponds to a total collagen concentration between 3 and 8 mg/mL [17,31]. Given a specific concentration of collagen, the ratio of PHYS to SPAAC collagen may then be modulated to adjust for the structural biomaterial stability required to counteract contraction forces exerted by encapsulated cells.

Furthermore, we expect that the collagen IPN could be adapted as a bioink for 3D bioprinting in order to create engineered tissue constructs with bespoke 3D geometries [91,92]. The lower molecular weight of the PEG-DBCO crosslinker (10 kDa) allows it to readily diffuse. Therefore, the SPAAC crosslinker can diffuse from the support bath used in embedded 3D bioprinting into the printed bioink, to covalently crosslink the SPAAC network component of the bioink after printing [17,93]. This would expand the potential for creating patient-specific collagen implants with tunable properties.

Overall, this collagen IPN offers a versatile foundation for developing hydrogel scaffolds that bridge the gap between cellular functionality and material stability to improve the efficacy and reliability of bioengineered collagen hydrogels.

5. Conclusions

In summary, we have developed an IPN based on two collagen networks that effectively integrates physical self-assembly (fibrillar, PHYS collagen) with covalent crosslinking (amorphous, SPAAC collagen). The unique crosslinking combination and microstructure of the collagen IPN promotes spreading of encapsulated cells without compromising bulk gel stability. By sequentially forming the IPN with (1) fibrillar, PHYS collagen and then (2) amorphous, SPAAC collagen to fill the interfibrillar space, we achieved a fibrillar microstructure similar to PHYS collagen alone. Importantly, this IPN was able to facilitate the spreading of encapsulated human corneal MSCs (like PHYS collagen alone) with negligible amounts of bulk gel contraction (like SPAAC collagen alone). While corneal cells were used as an exemplary cell type, we expect this collagen IPN to also be advantageous for other cell types and tissue applications that require local, dynamic cell-matrix interactions while preserving the bulk geometry of the biomaterial. Overall, our results suggest that this engineered collagen IPN holds significant potential for tissue engineering applications by promoting key cellular processes like spreading while preserving scaffold shape and stability.

Data availability

All data needed to evaluate the conclusions in the paper are present in the paper and/or the Supplementary Information. Data have also been deposited in the Stanford Digital Repository and can be accessed through the persistent URL (https://purl.stanford.edu/bg548vv5028) and the DOI (https://doi.org/10.25740/bg548vv5028).

CRediT authorship contribution statement

Lucia G. Brunel: Writing – review & editing, Writing – original draft, Visualization, Methodology, Investigation, Conceptualization. **Chris M. Long:** Writing – review & editing, Writing – original draft, Visualization, Methodology, Investigation, Conceptualization. **Fotis Christakopoulos:** Writing – review & editing, Methodology, Investigation. **Betty Cai:** Writing – review & editing, Methodology, Investigation. **Patrik K. Johansson:** Writing – review & editing, Methodology, Investigation. **Diya Singhal:** Writing – review & editing, Investigation. **Annika Enejder:** Writing – review & editing, Methodology. **David Myung:** Writing – review & editing, Supervision, Funding acquisition, Conceptualization. **Sarah C. Heilshorn:** Writing – review & editing, Writing – original draft, Supervision, Methodology, Funding acquisition, Conceptualization.

Declaration of competing interest

The authors declare that they have no known competing financial interests or personal relationships that could have appeared to influence the work reported in this paper.

The author is an Editorial Board Member/Editor-in-Chief/Associate Editor/Guest Editor for *Acta Biomaterialia* and was not involved in the editorial review or the decision to publish this article.

Acknowledgements

Graduate Fellowship in Science and Engineering (D.S.); a departmental core grant from Research to Prevent Blindness (D.M.), and the Advanced Research Projects Agency for Health including ARPA-H HEART (S.C.H).

Supplementary materials

Supplementary material associated with this article can be found, in the online version, at doi:10.1016/j.actbio.2025.01.009.

References

[1] B. Alberts, D. Bray, J. Lewis, M. Raff, K. Roberts, J.D. Watson, B. Alberts, D. Bray, J. Lewis, M. Raff, K. Roberts, J.D. Watson, Molecular Biology of the Cell, 3rd ed., Garland Science, 1994.

[2] R. Parenteau-Bareil, R. Gauvin, F. Berthod, Collagen-Based biomaterials for tissue engineering applications, Materials (Basel) 3 (2010) 1863–1887, https://doi.org/10.3390/ma3031863.

[3] G. Charriere, M. Bejot, L. Schnitzler, G. Ville, D.J. Hartmann, Reactions to a bovine collagen implant. Clinical and immunologic study in 705 patients, J. Am. Acad. Dermatol. 21 (1989) 1203–1208, https://doi.org/10.1016/s0190-9622(89)70330-3.

[4] S.I. Fraley, P.-H. Wu, L. He, Y. Feng, R. Krisnamurthy, G.D. Longmore, D. Wirtz, Three-dimensional matrix fiber alignment modulates cell migration and MT1-MMP utility by spatially and temporally directing protrusions, Sci. Rep. 5 (2015) 14580, https://doi.org/10.1038/srep14580.

[5] H.C. Pruitt, D. Lewis, M. Ciccaglione, S. Connor, Q. Smith, J.W. Hickey, J. P. Schneck, S. Gerecht, Collagen fiber structure guides 3D motility of cytotoxic T lymphocytes, Matrix Biol. 85–86 (2020) 147–159, https://doi.org/10.1016/j.matbio.2019.02.003.

[6] J. Sapudom, S. Karaman, B.C. Quartey, W.K.E. Mohamed, N. Mahtani, A. Garcia-Sabaté, J. Teo, Collagen fibril orientation instructs fibroblast differentiation via cell contractility, Adv. Sci. (Weinh) 10 (2023) e2301353, https://doi.org/10.1002/advs.202301353.

[7] K.M. Yamada, A.D. Doyle, J. Lu, Cell–3D matrix interactions: recent advances and opportunities, Trends Cell Biol. 32 (2022) 883–895, https://doi.org/10.1016/j.tcb.2022.03.002.

[8] M.F. Goody, C.A. Henry, Dynamic interactions between cells and their extracellular matrix mediate embryonic development, Mol. Reprod. Dev. 77 (2010) 475–488, https://doi.org/10.1002/mrd.21157.

[9] J.M. Grolman, P. Weinand, D.J. Mooney, Extracellular matrix plasticity as a driver of cell spreading, Proc. Natl. Acad. Sci. U.S.A. 117 (2020) 25999–26007, https://doi.org/10.1073/pnas.2008801117.

[10] S. Nam, J. Lee, D.G. Brownfield, O. Chaudhuri, Viscoplasticity enables mechanical remodeling of matrix by cells, Biophys. J. 111 (2016) 2296–2308, https://doi.org/10.1016/j.bpj.2016.10.002.

[11] B. Wehrle-Haller, Assembly and disassembly of cell matrix adhesions, Curr. Opin. Cell Biol. 24 (2012) 569–581, https://doi.org/10.1016/j.ceb.2012.06.010.

[12] A. Bajpai, J. Tong, W. Qian, Y. Peng, W. Chen, The interplay between cell-cell and cell-matrix forces regulates cell migration dynamics, Biophys. J. 117 (2019) 1795–1804, https://doi.org/10.1016/j.bpj.2019.10.015.

[13] T. Zhang, J.H. Day, X. Su, A.G. Guadarrama, N.K. Sandbo, S. Esnault, L. C. Denlinger, E. Berthier, A.B. Theberge, Investigating fibroblast-induced collagen gel contraction using a dynamic microscale platform, Front. Bioeng. Biotechnol. 7 (2019) 196, https://doi.org/10.3389/fbioe.2019.00196.

[14] F. Grinnell, Fibroblast-collagen-matrix contraction: growth-factor signalling and mechanical loading, Trends. Cell Biol. 10 (2000) 362–365, https://doi.org/10.1016/s0962-8924(00)01802-x.

[15] X. Wang, Q. Gao, X. Han, B. Bu, L. Wang, A. Li, L. Deng, Sensitive detection of cell-derived force and collagen matrix tension in microtissues undergoing large-scale densification, Proc. Natl. Acad. Sci. U.S.A. 118 (2021) e2106061118, https://doi.org/10.1073/pnas.2106061118.

[16] M. Machour, N. Hen, I. Goldfracht, D. Safina, M. Davidovich-Pinhas, H. Bianco-Peled, S. Levenberg, Print-and-Grow within a novel support material for 3D bioprinting and post-printing tissue growth, Adv. Sci. (Weinh) 9 (2022) e2200882, https://doi.org/10.1002/advs.202200882.

[17] L.G. Brunel, F. Christakopoulos, D. Kilian, B. Cai, S.M. Hull, D. Myung, S. C. Heilshorn, Embedded 3D bioprinting of collagen inks into microgel baths to control hydrogel microstructure and cell spreading, Adv. Healthc. Mater. (2023) e2303325, https://doi.org/10.1002/adhm.202303325.

[18] C. Lotz, F.F. Schmid, E. Oechsle, M.G. Monaghan, H. Walles, F. Groeber-Becker, Cross-linked collagen hydrogel matrix resisting contraction to facilitate full-thickness skin equivalents, ACS. Appl. Mater. Interfaces 9 (2017) 20417–20425, https://doi.org/10.1021/acsami.7b04017.

[19] S.A. Hilton, L.C. Dewberry, M.M. Hodges, J. Hu, J. Xu, K.W. Liechty, C. Zgheib, Mesenchymal stromal cells contract collagen more efficiently than dermal fibroblasts: implications for cytotherapy, PLoS One 14 (2019) e0218536, https://doi.org/10.1371/journal.pone.0218536.

[20] E. Bell, B. Ivarsson, C. Merrill, Production of a tissue-like structure by contraction of collagen lattices by human fibroblasts of different proliferative potential *in vitro*, Proc. Natl. Acad. Sci. u S a 76 (1979) 1274–1278.

[21] Y.-H. Jiang, Y.-Y. Lou, T.-H. Li, B.-Z. Liu, K. Chen, D. Zhang, T. Li, Cross-linking methods of type I collagen-based scaffolds for cartilage tissue engineering, Am. J. Transl. Res. 14 (2022) 1146–1159.

[22] M.-T. Sheu, J.-C. Huang, G.-C. Yeh, H.-O. Ho, Characterization of collagen gel solutions and collagen matrices for cell culture, Biomaterials 22 (2001) 1713–1719, https://doi.org/10.1016/S0142-9612(00)00315-X.

[23] D.V. Shepherd, J.H. Shepherd, S. Ghose, S.J. Kew, R.E. Cameron, S.M. Best, The process of EDC-NHS Cross-linking of reconstituted collagen fibres increases collagen fibrillar order and alignment, APL Mater. 3 (2015) 014902, https://doi.org/10.1063/1.4900887.

[24] J.C. Ashworth, M. Mehr, P.G. Buxton, S.M. Best, R.E. Cameron, Cell invasion in collagen scaffold architectures characterized by percolation theory, Adv. Healthc. Mater. 4 (2015) 1317–1321, https://doi.org/10.1002/adhm.201500197.

[25] Y. Abbas, L.G. Brunel, M.S. Hollinshead, R.C. Fernando, L. Gardner, I. Duncan, A. Moffett, S. Best, M.Y. Turco, G.J. Burton, R.E. Cameron, Generation of a three-dimensional collagen scaffold-based model of the human endometrium, Interface Focus 10 (2020) 20190079, https://doi.org/10.1098/rsfs.2019.0079.

[26] C.M. Madl, S.C. Heilshorn, Bioorthogonal strategies for engineering extracellular matrices, Adv. Funct. Mater. 28 (2018) 1706046, https://doi.org/10.1002/adfm.201706046.

[27] N.J. Agard, J.A. Prescher, C.R. Bertozzi, A strain-promoted [3 + 2] Azide−Alkyne cycloaddition for covalent modification of biomolecules in living systems, J. Am. Chem. Soc. 126 (2004) 15046–15047, https://doi.org/10.1021/ja044996f.

[28] H.J. Lee, G.M. Fernandes-Cunha, K.-S. Na, S.M. Hull, D. Myung, Bio-Orthogonally crosslinked, in situ forming corneal stromal tissue substitute, Adv. Healthc. Mater. 7 (2018) e1800560, https://doi.org/10.1002/adhm.201800560.

[29] Y. Liu, L. Gan, D.J. Carlsson, P. Fagerholm, N. Lagali, M.A. Watsky, R. Munger, W. G. Hodge, D. Priest, M. Griffith, A simple, cross-linked collagen tissue substitute for corneal implantation, Invest. Ophthalmol. Vis. Sci. 47 (2006) 1869–1875, https://doi.org/10.1167/iovs.05-1339.

[30] G.M. Fernandes-Cunha, K.M. Chen, F. Chen, P. Le, J.H. Han, L.A. Mahajan, H. J. Lee, K.S. Na, D. Myung, In situ-forming collagen hydrogel crosslinked via multi-functional PEG as a matrix therapy for corneal defects, Sci. Rep. 10 (2020) 16671, https://doi.org/10.1038/s41598-020-72978-5.

[31] L.G. Brunel, B. Cai, S.M. Hull, U. Han, T. Wungcharoen, G.M. Fernandes-Cunha, Y. A. Seo, P.K. Johansson, S.C. Heilshorn, D. Myung, In Situ UNIversal Orthogonal Network (UNION) Bioink Deposition for Direct Delivery of Corneal Stromal Stem Cells to Corneal Wounds, (2024) 2024.09.19.613997. https://doi.org/10.1101/2024.09.19.613997.

[32] J.A. West-Mays, D.J. Dwivedi, The keratocyte: corneal stromal cell with variable repair phenotypes, Int. J. Biochem. Cell Biol. 38 (2006) 1625–1631, https://doi.org/10.1016/j.biocel.2006.03.010.

[33] G. Montalbano, S. Toumpaniari, A. Popov, P. Duan, J. Chen, K. Dalgarno, W. E. Scott, A.M. Ferreira, Synthesis of bioinspired collagen/alginate/fibrin based hydrogels for soft tissue engineering, Mater. Sci. Eng. C 91 (2018) 236–246, https://doi.org/10.1016/j.msec.2018.04.101.

[34] R. Mahou, A.E. Vlahos, A. Shulman, M.V. Sefton, Interpenetrating alginate-collagen polymer network microspheres for modular tissue engineering, ACS Biomater. Sci. Eng. 4 (2018) 3704–3712, https://doi.org/10.1021/acsbiomaterials.7b00356.

[35] M. Bernero, D. Zauchner, R. Müller, X.-H. Qin, Interpenetrating network hydrogels for studying the role of matrix viscoelasticity in 3D osteocyte morphogenesis, Biomater. Sci. 12 (2024) 919–932, https://doi.org/10.1039/D3BM01781H.

[36] J. Lou, R. Stowers, S. Nam, Y. Xia, O. Chaudhuri, Stress relaxing hyaluronic acid-collagen hydrogels promote cell spreading, fiber remodeling, and focal adhesion formation in 3D cell culture, Biomaterials 154 (2018) 213–222, https://doi.org/10.1016/j.biomaterials.2017.11.004.

[37] J. Dommerholt, F.P.J.T. Rutjes, F.L. van Delft, Strain-Promoted 1,3-dipolar cycloaddition of cycloalkynes and organic azides, Top. Curr. Chem. (Z) 374 (2016) 16, https://doi.org/10.1007/s41061-016-0016-4.

[38] P. Jönsson, M.P. Jonsson, J.O. Tegenfeldt, F. Höök, A method improving the accuracy of fluorescence recovery after photobleaching analysis, Biophys. J. 95 (2008) 5334–5348, https://doi.org/10.1529/biophysj.108.134874.

[39] S. Jabbehdari, G. Yazdanpanah, L.N. Kanu, K.N. Anwar, X. Shen, B. Rabiee, I. Putra, M. Eslani, M.I. Rosenblatt, P. Hematti, A.R. Djalilian, Reproducible derivation and expansion of corneal mesenchymal stromal cells for therapeutic applications, Transl. Vis. Sci. Technol. 9 (2020) 26, https://doi.org/10.1167/tvst.9.3.26.

[40] J. Schindelin, I. Arganda-Carreras, E. Frise, V. Kaynig, M. Longair, T. Pietzsch, S. Preibisch, C. Rueden, S. Saalfeld, B. Schmid, J.-Y. Tinevez, D.J. White, V. Hartenstein, K. Eliceiri, P. Tomancak, A. Cardona, Fiji: an open-source platform for biological-image analysis, Nat. Methods 9 (2012) 676–682, https://doi.org/10.1038/nmeth.2019.

[41] N.S. Rossen, A. Kyrsting, A.J. Giaccia, J.T. Erler, L.B. Oddershede, Fiber finding algorithm using stepwise tracing to identify biopolymer fibers in noisy 3D images, Biophys. J. 120 (2021) 3860–3868, https://doi.org/10.1016/j.bpj.2021.08.017.

[42] N. Otsu, A threshold selection method from gray-level histograms, IEEE Trans. Syst. Man Cybern. 9 (1979) 62–66.

[43] B.M. Baker, C.S. Chen, Deconstructing the third dimension: how 3D culture microenvironments alter cellular cues, J. Cell Sci. 125 (2012) 3015–3024, https://doi.org/10.1242/jcs.079509.

[44] K.H. Vining, D.J. Mooney, Mechanical forces direct stem cell behaviour in development and regeneration, Nat. Rev. Mol. Cell Biol. 18 (2017) 728–742, https://doi.org/10.1038/nrm.2017.108.

[45] D.L. Christiansen, E.K. Huang, F.H. Silver, Assembly of type I collagen: fusion of fibril subunits and the influence of fibril diameter on mechanical properties, Matrix Biol. 19 (2000) 409–420, https://doi.org/10.1016/s0945-053x(00)00089-5.

[46] D. Rütsche, M. Nanni, S. Rüdisser, T. Biedermann, M. Zenobi-Wong, Enzymatically crosslinked collagen as a versatile matrix for in vitro and in vivo Co-engineering of

blood and lymphatic vasculature, Adv. Mater. 35 (2023) 2209476, https://doi.org/10.1002/adma.202209476.

[47] I.D. Gaudet, D.I. Shreiber, Characterization of methacrylated type-I collagen as a dynamic, photoactive hydrogel, Biointerphases. 7 (2012) 25, https://doi.org/10.1007/s13758-012-0025-y.

[48] C.N. Grover, J.H. Gwynne, N. Pugh, S. Hamaia, R.W. Farndale, S.M. Best, R.E. Cameron, Crosslinking and composition influence the surface properties, mechanical stiffness and cell reactivity of collagen-based films, Acta Biomater. 8 (2012) 3080–3090, https://doi.org/10.1016/j.actbio.2012.05.006.

[49] D. Myung, D. Waters, M. Wiseman, P.-E. Duhamel, J. Noolandi, C.N. Ta, C.W. Frank, Progress in the development of interpenetrating polymer network hydrogels, Polym. Adv. Technol. 19 (2008) 647–657, https://doi.org/10.1002/pat.1134.

[50] E.S. Dragan, Design and applications of interpenetrating polymer network hydrogels. A review, Chem. Eng. J. 243 (2014) 572–590, https://doi.org/10.1016/j.cej.2014.01.065.

[51] C.O. Crosby, B. Stern, N. Kalkunte, S. Pedahzur, S. Ramesh, J. Zoldan, Interpenetrating polymer network hydrogels as bioactive scaffolds for tissue engineering, Rev. Chem. Eng. 38 (2022) 347–361, https://doi.org/10.1515/revce-2020-0039.

[52] M.G.T.A. Rutten, L. Rijns, P.Y.W. Dankers, Controlled, supramolecular polymer formulation to engineer hydrogels with tunable mechanical and dynamic properties, J. Polym. Sci. 62 (2024) 155–164, https://doi.org/10.1002/pol.20230283.

[53] O. Chaudhuri, Viscoelastic hydrogels for 3D cell culture, Biomater. Sci. 5 (2017) 1480–1490, https://doi.org/10.1039/C7BM00261K.

[54] O. Chaudhuri, J. Cooper-White, P.A. Janmey, D.J. Mooney, V.B. Shenoy, Effects of extracellular matrix viscoelasticity on cellular behaviour, Nature 584 (2020) 535–546, https://doi.org/10.1038/s41586-020-2612-2.

[55] B. Yi, Q. Xu, W. Liu, An overview of substrate stiffness guided cellular response and its applications in tissue regeneration, Bioact. Mater. 15 (2021) 82–102, https://doi.org/10.1016/j.bioactmat.2021.12.005.

[56] A.J. Bailey, J. Macmillan, P.R. Shrewry, A.S. Tatham, R. Puxkandl, I. Zizak, O. Paris, J. Keckes, W. Tesch, S. Bernstorff, P. Purslow, P. Fratzl, Viscoelastic properties of collagen: synchrotron radiation investigations and structural model, Philos. Trans. R. Soc. London Ser. B Biol. Sci. 357 (2002) 191–197, https://doi.org/10.1098/rstb.2001.1033.

[57] O. Chaudhuri, L. Gu, D. Klumpers, M. Darnell, S.A. Bencherif, J.C. Weaver, N. Huebsch, H. Lee, E. Lippens, G.N. Duda, D.J. Mooney, Hydrogels with tunable stress relaxation regulate stem cell fate and activity, Nat. Mater. 15 (2016) 326–334, https://doi.org/10.1038/nmat4489.

[58] S. Nam, K.H. Hu, M.J. Butte, O. Chaudhuri, Strain-enhanced stress relaxation impacts nonlinear elasticity in collagen gels, Proc. Natl. Acad. Sci. 113 (2016) 5492–5497, https://doi.org/10.1073/pnas.1523906113.

[59] F. Yang, D. Das, K. Karunakaran, G.M. Genin, S. Thomopoulos, I. Chasiotis, Nonlinear time-dependent mechanical behavior of mammalian collagen fibrils, Acta Biomater. 163 (2023) 63–77, https://doi.org/10.1016/j.actbio.2022.03.005.

[60] M. Marenzana, D. Pickard, A.J. MacRobert, R.A. Brown, Optical measurement of three-dimensional collagen gel constructs by elastic scattering spectroscopy, Tissue Eng. 8 (2002) 409–418, https://doi.org/10.1089/107632702760184673.

[61] J.M. Gordon, E.A. Bauer, A.Z. Eisen, Collagenase in human cornea: immunologic localization, Arch. Ophthalmol. 98 (1980) 341–345, https://doi.org/10.1001/archopht.1980.01020030337022.

[62] W.Y. Wang, C.D. Davidson, D. Lin, B.M. Baker, Actomyosin contractility-dependent matrix stretch and recoil induces rapid cell migration, Nat. Commun. 10 (2019) 1186, https://doi.org/10.1038/s41467-019-09121-0.

[63] Q. Li, Y. Zhang, P. Pluchon, J. Robens, K. Herr, M. Mercade, J.-P. Thiery, H. Yu, V. Viasnoff, Extracellular matrix scaffolding guides lumen elongation by inducing anisotropic intercellular mechanical tension, Nat. Cell Biol. 18 (2016) 311–318, https://doi.org/10.1038/ncb3310.

[64] Y. Du, M.L. Funderburgh, M.M. Mann, N. SundarRaj, J.L. Funderburgh, Multipotent stem cells in human corneal stroma, Stem Cells 23 (2005) 1266–1275, https://doi.org/10.1634/stemcells.2004-0256.

[65] J.L. Funderburgh, M.L. Funderburgh, Y. Du, Stem cells in the limbal stroma, Ocul. Surf. 14 (2016) 113–120, https://doi.org/10.1016/j.jtos.2015.12.006.

[66] J. Ruiz-Franco, J. van Der Gucht, Force transmission in disordered fibre networks, Front. Cell Dev. Biol. 10 (2022), https://doi.org/10.3389/fcell.2022.931776.

[67] S.O. Sarrigiannidis, J.M. Rey, O. Dobre, C. González-García, M.J. Dalby, M. Salmeron-Sanchez, A tough act to follow: collagen hydrogel modifications to improve mechanical and growth factor loading capabilities, Mater. Today Bio. 10 (2021) 100098, https://doi.org/10.1016/j.mtbio.2021.100098.

[68] L. Han, J. Lin, C. Du, C. Zhang, X. Wang, Q. Feng, Effect of mechanical microenvironment on collagen self-assembly in vitro, J. Funct. Biomater. 14 (2023) 235, https://doi.org/10.3390/jfb14040235.

[69] X. Song, Z. Wang, S. Tao, G. Li, J. Zhu, Observing effects of calcium/magnesium Ions and pH value on the self-assembly of extracted swine tendon collagen by atomic force microscopy, J Food Qual 2017 (2017) 9257060, https://doi.org/10.1155/2017/9257060.

[70] J. Stepanovska, M. Supova, K. Hanzalek, A. Broz, R. Matejka, Collagen bioinks for bioprinting: a systematic review of hydrogel properties, bioprinting parameters, protocols, and bioprinted structure characteristics, Biomedicines 9 (2021) 1137, https://doi.org/10.3390/biomedicines9091137.

[71] L. Bi, Z. Cao, Y. Hu, Y. Song, L. Yu, B. Yang, J. Mu, Z. Huang, Y. Han, Effects of different cross-linking conditions on the properties of genipin-cross-linked chitosan/collagen scaffolds for cartilage tissue engineering, J. Mater. Sci. Mater. Med. 22 (2011) 51–62, https://doi.org/10.1007/s10856-010-4177-3.

[72] Y.-J. Hwang, J. Larsen, T.B. Krasieva, J.G. Lyubovitsky, Effect of genipin crosslinking on the optical spectral properties and structures of collagen hydrogels, ACS Appl. Mater. Interfaces 3 (2011) 2579–2584, https://doi.org/10.1021/am200416h.

[73] G. Da Silva André, C. Labouesse, Mechanobiology of 3D cell confinement and extracellular crowding, Biophys. Rev. (2024), https://doi.org/10.1007/s12551-024-01244-z.

[74] K.L. Xu, N. Di Caprio, H. Fallahi, M. Dehghany, M.D. Davidson, L. Laforest, B.C.H. Cheung, Y. Zhang, M. Wu, V. Shenoy, L. Han, R.L. Mauck, J.A. Burdick, Microinterfaces in biopolymer-based bicontinuous hydrogels guide rapid 3D cell migration, Nat. Commun. 15 (2024) 2766, https://doi.org/10.1038/s41467-024-46774-y.

[75] S. Perumal, O. Antipova, J.P.R.O. Orgel, Collagen fibril architecture, domain organization, and triple-helical conformation govern its proteolysis, Proc. Natl. Acad. Sci. U.S.A. 105 (2008) 2824–2829, https://doi.org/10.1073/pnas.0710588105.

[76] J.P.R.O. Orgel, J.D. San Antonio, O. Antipova, Molecular and structural mapping of collagen fibril interactions, Connect. Tissue Res. 52 (2011) 2–17, https://doi.org/10.3109/03008207.2010.511353.

[77] I. Mercier, J.-P. Lechaire, A. Desmouliere, F. Gaill, M. Aumailley, Interactions of human skin fibroblasts with monomeric or fibrillar collagens induce different organization of the cytoskeleton, Exp. Cell Res. 225 (1996) 245–256, https://doi.org/10.1006/excr.1996.0174.

[78] S. Manzano, R. Moreno-Loshuertos, M. Doblaré, I. Ochoa, M.H. Doweidar, Structural biology response of a collagen hydrogel synthetic extracellular matrix with embedded human fibroblast: computational and experimental analysis, Med. Biol. Eng. Comput. 53 (2015) 721–735, https://doi.org/10.1007/s11517-015-1277-8.

[79] N. Zhang, Y. Cheng, X. Hu, J. Yeo, Toward rational algorithmic design of collagen-based biomaterials through multiscale computational modeling, Curr. Opin. Chem. Eng. 24 (2019) 79–87, https://doi.org/10.1016/j.coche.2019.02.011.

[80] J.F. Eichinger, M.J. Grill, I.D. Kermani, R.C. Aydin, W.A. Wall, J.D. Humphrey, C.J. Cyron, A computational framework for modeling cell–matrix interactions in soft biological tissues, Biomech. Model. Mechanobiol. 20 (2021) 1851–1870, https://doi.org/10.1007/s10237-021-01480-2.

[81] C. Dong, Y. Lv, Application of collagen scaffold in tissue engineering: recent advances and new perspectives, Polymers (Basel) 8 (2016) 42, https://doi.org/10.3390/polym8020042.

[82] J. Zhu, Z. Li, Y. Zou, G. Lu, A. Ronca, U. D'Amora, J. Liang, Y. Fan, X. Zhang, Y. Sun, Advanced application of collagen-based biomaterials in tissue repair and restoration, J. Leather Sci. Eng. 4 (2022) 30, https://doi.org/10.1186/s42825-022-00102-6.

[83] D.A. Newsome, J.M. Foidart, J.R. Hassell, J.H. Krachmer, M.M. Rodrigues, S.I. Katz, Detection of specific collagen types in normal and keratoconus corneas, Invest. Ophthalmol. Vis. Sci. 20 (1981) 738–750.

[84] K.M. Meek, Corneal collagen—Its role in maintaining corneal shape and transparency, Biophys. Rev. 1 (2009) 83–93, https://doi.org/10.1007/s12551-009-0011-x.

[85] E.M. Espana, D.E. Birk, Composition, structure and function of the corneal stroma, Exp. Eye Res. 198 (2020) 108137, https://doi.org/10.1016/j.exer.2020.108137.

[86] Y. Du, E.C. Carlson, M.L. Funderburgh, D.E. Birk, E. Pearlman, N. Guo, W.W.-Y. Kao, J.L. Funderburgh, Stem cell therapy restores transparency to defective murine corneas, Stem Cells 27 (2009) 1635–1642, https://doi.org/10.1002/stem.91.

[87] T. Volatier, C. Cursiefen, M. Notara, Current advances in corneal stromal stem cell biology and therapeutic applications, Cells 13 (2024) 163, https://doi.org/10.3390/cells13020163.

[88] E.V. Shvetsova, O.S. Rogovaya, S.B. Tkachenko, I.V. Kiselev, A.V. Vasil'ev, V.V. Terskikh, Contractile capacity of fibroblasts from different sources in the model of living skin equivalent, Biol. Bull. Russ. Acad. Sci. 35 (2008) 146–150, https://doi.org/10.1134/S1062359008020088.

[89] S. Yin, X. Zhang, C. Zhan, J. Wu, J. Xu, J. Cheung, Measuring single cardiac myocyte contractile force via moving a magnetic bead, Biophys. J. 88 (2005) 1489–1495, https://doi.org/10.1529/biophysj.104.048157.

[90] R.J. Adams, A. Schwartz, Comparative mechanisms for contraction of cardiac and skeletal muscle, Chest 78 (1980) 123–139, https://doi.org/10.1378/chest.78.1_Supplement.123.

[91] S.M. Hull, L.G. Brunel, S.C. Heilshorn, 3D Bioprinting of cell-laden hydrogels for improved biological functionality, Adv. Mater. 34 (2022) e2103691, https://doi.org/10.1002/adma.202103691.

[92] L.G. Brunel, S.M. Hull, S.C. Heilshorn, Engineered assistive materials for 3D bioprinting: support baths and sacrificial inks, Biofabrication 14 (2022), https://doi.org/10.1088/1758-5090/ac6bbe.

[93] S.M. Hull, C.D. Lindsay, L.G. Brunel, D.J. Shiwarski, J.W. Tashman, J.G. Roth, D. Myung, A.W. Feinberg, S.C. Heilshorn, 3D Bioprinting using UNIversal orthogonal network (UNION) bioinks, Adv. Funct. Mater. 31 (2021) 2007983, https://doi.org/10.1002/adfm.202007983.